



MONASH
University

School of Physics and Astronomy/Astrophysics

HONOURS THESIS

**Close Packing of Lund Strings and its
Effects on Strangeness Enhancement**

Javira Altmann

ID: 2969 8537

Supervised by : Peter Skands

Date: November 2021

Abstract

The data provided by the ALICE collaboration at the LHC [1] shows a rise in strange quark production with respect to the charged particle multiplicity in pp collisions. The Monte-Carlo event generator PYTHIA [2, 3], using its default tune Monash 2013 [4], cannot describe this data and instead predicts constant strangeness. Hence we introduce a mechanism called “close packing” [5], which is invoked during the hadronisation process using the Lund String model [6]. Close packing is a collective effect which alters the string tension of a given string due to many strings residing in the same vicinity. From implementing this mechanism in PYTHIA, we are able to successfully predict a rise in strangeness. Though further work remains, the results are promising and certainly warrant further investigation.

Acknowledgements

I would like to say a special thank you to Peter Skands for being an incredibly supportive supervisor. I thank him for the extremely invaluable guidance and feedback throughout the project, as well as his patience and advice throughout the year. I also extend thanks to Christian Holm Christensen for his explanations of primary particles and the event classes used to describe dependence on charged particle multiplicity in the ALICE analyses, as well as Christian Bierlich for his suggestions on hadron rescattering.

Contents

1	Introduction	5
1.1	Overview of QCD	6
1.1.1	Large N_c limit	7
1.1.2	MPIs and Colour Reconnections	7
2	Lund String Model	10
2.1	String Fundamentals	10
2.1.1	Fragmentation and Jet Production	11
2.1.2	String Diagrams	13
2.2	Schwinger Mechanism	15
2.3	Symmetric Fragmentation Function	16
2.4	Lambda measure	17
2.5	Junctions	17
3	Close Packing	20
4	Implementation in PYTHIA	24
4.1	Probabilities	24
4.2	p_\perp Distribution	26
4.3	PYTHIA Functions	26
5	Results	27
5.1	ALICE Strangeness Data	28
5.2	Model Efficiency	32
5.3	CMS Observables	33
5.4	Remaining Issues	37
5.4.1	Baryon production	37
5.4.2	Hadron rescattering	38
6	Summary and Outlook	41
	References	43
A	Model Parameters	46
B	Diquark to quark probability	49

C	PYTHIA code	50
C.1	rapidityPairs in HadronLevel.cc	50
C.2	kappaEffectiveRatio in StringFragmentation.cc	52
C.3	Reinitialisation of Probabilities in FragmentationFlavZpT.cc	55
D	ALICE Analysis	56

1 Introduction

In high-energy collisions such as e^+e^- and pp (and more generally hadron-hadron) collisions, like those at the Large Hadron Collider (LHC), hadrons are created in clusters about some small polar and azimuthal angle, forming cone-like “jets” of hadrons as seen in Figure 1.1. In order to fully describe the event structure of hadronic final states from such collisions, many different quantum chromodynamic (QCD) effects must be considered, including both “hard” perturbative and “soft” non-perturbative processes. The key focus of this thesis is the non-perturbative process of hadronisation.

The Lund String Model [7] is a semi-classical phenomenological model for long-range QCD, where the breaking (fragmentation) of the strings attempts to model the hadronisation process. It is one of the most widely used formulations for modelling hadronisation in high-energy collisions, and is the model explored in this paper.

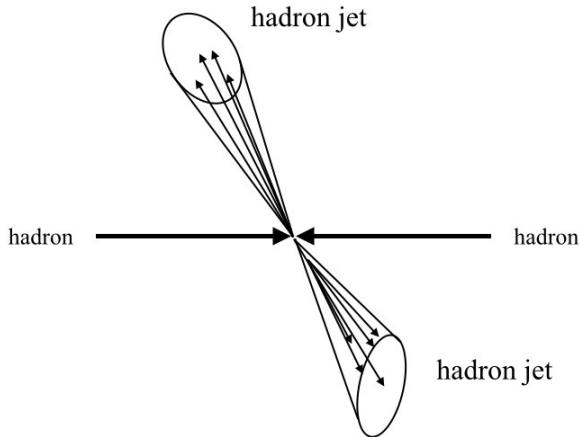


Figure 1.1. A simple visual representation showing the jet structure resulting from a hadron-hadron collision.

A defining feature of strings is the constant string tension, κ , which corresponds to a potential with constant slope κ . Thus a strong motivation for a string model is the Cornell potential [8, 9], which is determined by lattice QCD and models the static QCD potential between a quark and an antiquark in an overall colour-singlet state (explained in Section 1.1 below). At distances of $r \gtrsim 1$ fm, the Cornell potential follows a linear potential, and thus leads to the long-range QCD string model.

1.1 Overview of QCD

QCD is represented by the $SU(3)$ gauge group. Elements of the $SU(3)$ group are the set of unitary 3×3 matrices with a determinant of one, resulting in 8 different generators corresponding to the 8 independent directions in matrix space. These generators are represented by Gell-Mann matrices (see ref. [10]), which are traceless and hermitian, and are analogous to the well known Pauli matrices in $SU(2)$.

The $SU(3)$ group represents the “colour space” of QCD. Within this colour space, there are three colour charges; red (R), green (G) and blue (B), and three corresponding anticolour charges; \bar{R} , \bar{G} and \bar{B} .

Quarks (q) are $SU(3)$ triplets, which are a linear superposition of R, G and B . Likewise antiquarks (\bar{q}) are $SU(3)$ antitriplets which are a linear superposition of \bar{R}, \bar{G} and \bar{B} . Gluons (g) are in the octet (adjoint) representation of the $SU(3)$ group, and carry both a colour and an anticolour charge however cannot be a colourless state. Thus gluons can “repaint” quarks (see Figure 1.2), and gluon self interactions can occur, including gluon loops. Colour flow is the QCD analog to charge flow in QED. Colour flow determines the string topology in the Lund string model. Likewise, analogous to charge conservation in QED, QCD also has colour charge conserved.

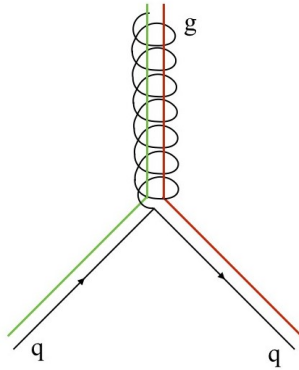


Figure 1.2. A qgq vertex showing colour flow, with a quark carrying a red colour charge, a quark carrying a green colour charge, and the gluon carrying both red and green colour charges.

A key feature of QCD is confinement, which states that free particles are found in colourless (colour-singlet) bound states, otherwise known as hadrons. This limits the

form of hadronic final states possible. As an example, a $q\bar{q}$ pair can exist as a free particle as it corresponds to $3 \otimes \bar{3} = 8 \oplus 1$, which includes a singlet state. On the other hand, qq pair cannot exist as free particle as $3 \otimes 3 = 6 \oplus \bar{3}$ contains no singlet state. The two simplest types of hadrons are mesons and baryons. Mesons are comprised of a quark and antiquark, and (anti)baryons are comprised of three (anti)quarks.

1.1.1 Large N_c limit

Although QCD is a finite gauge theory, namely $SU(3)$, it is often generalised to a N_c gauge theory, $SU(N_c)$, so that a large N_c limit can be taken. This is usually referred to as the leading colour (LC) limit. In this limit each parton has a unique colour, which can simplify the treatment of colour in event generators such as Monte-Carlo simulations (see [10] for further detail on Monte-Carlo event generators).

The combination of a colour and anticolour, using group theory, gives an adjoint colour and colour singlet according to $N_c \otimes \bar{N}_c = (N_c^2 - 1) \oplus 1$. In the large N_c limit, the singlet state is ignored (i.e. $N_c \otimes \bar{N}_c \sim (N_c^2 - 1)$), resulting in corrections that are expected to be suppressed by $1/N_c^2 \sim 10\%$ (using $N_c = 3$). Often the dynamical suppression is greater due to topological constraints.

1.1.2 MPIs and Colour Reconnections

In order to understand the close packing mechanism, we need a complete understanding of the hadronisation process including how these string configurations are formed. The initial configuration of hadronising strings is determined by so-called MPIs and colour reconnections. Due to the composite nature of hadrons, in a single hadron-hadron collision several partonic collisions may occur, leading to several “multi-parton interaction (MPI) systems” where an MPI system is defined as a collision between two partons. In the LC limit, each final-state parton is colour-connected to a single other parton uniquely. This means that the set of connections that define the string are unique, resulting in each MPI system hadronising independently.

Colour reconnections (CR) is a broad term which is used to refer to physical effects beyond the LC limit that can alter between which partons confining potentials arise, and occur when they offer more favourable configurations; with less energy or “shorter” string lengths (see the lambda measure in Section 2.4 for more on string

lengths). Broadly, one may distinguish between two classes of CR effects; colour-space ambiguities and dynamical reconfigurations.

Colour-space ambiguity allows for multiple partons to potentially carry identical colours. As colour space is a finite gauge theory, there is thus a probability to have “colour accidents”. These colour accidents occur when there are multiple partons carrying the same colour charge resulting in multiple possible string topologies.

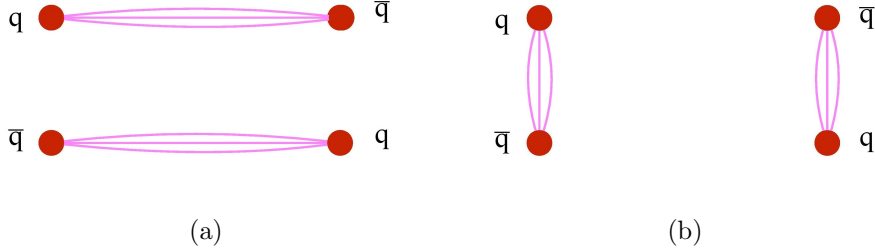


Figure 1.3. Two possible string topologies for the given colour configurations. (a) String configuration before CR effects. (b) Alternative topology allowed by CR.

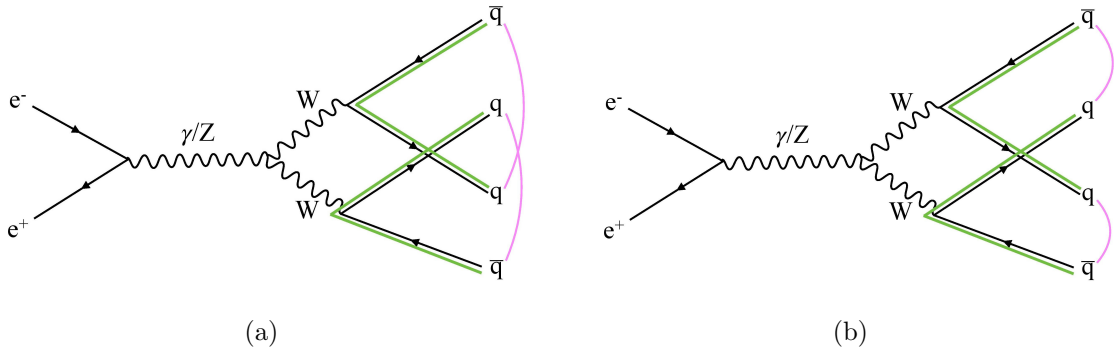


Figure 1.4. Feynman diagrams showing an $ee \rightarrow WW$ process where each W boson decays into a $q\bar{q}$ pair. The green lines indicate colour flow, where colours are represented above the feynman diagram lines, and anticolours are represented below them. (a) Before CR effects, with the string stretched between each quark-antiquark pair as they are created. (b) After CR effects are allowed, showing an alternative string configuration whilst still ensuring colour singlet final states.

Consider the simple example of two quark dipoles as shown in Figure 1.3. In the LC limit, the strings have unique configurations as each parton has a unique colour. However, given a finite N_c , there is a finite probability that the partons “accidentally” have the same colour, say red-antired. Figure 1.3 demonstrates two possible different string configurations for such a scenario. Figure 1.4 shows CR in the context of an e^+e^- collision.

In the context of pp collisions, confining potentials are formed between a jet and each beam remnant as seen in Figure 1.5 (a). Contrastingly, with CR effects, the confining potentials can form between jets and then connect back to the beam remnant, rather than each jet being independently connected to the beam remnant, illustrated in Figure 1.5 (b).

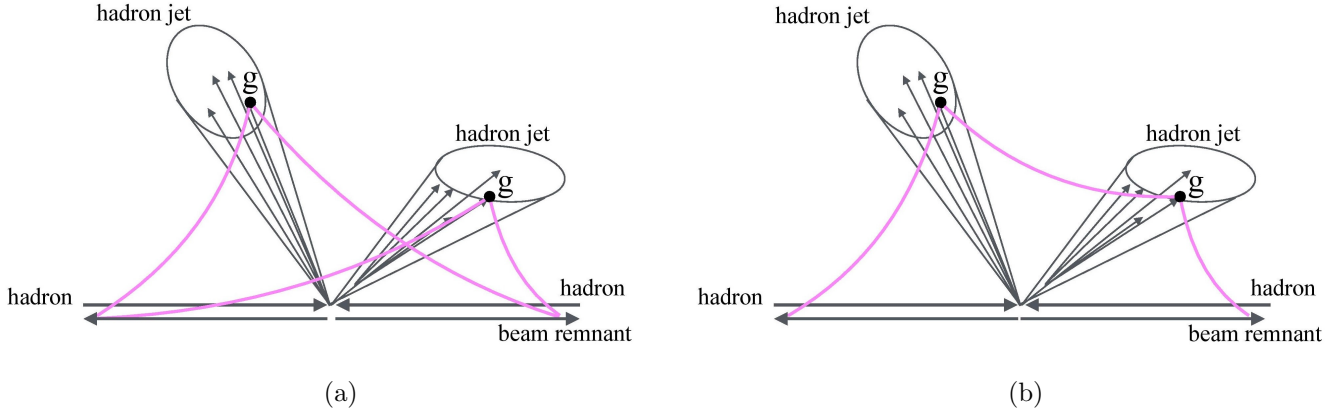


Figure 1.5. (a) The string topology ignoring CR effects, where strings are formed directly between the beam remnant and the jet. (b) Allowing for CR effects, the dynamically favourable string configuration. The string is now spanned from the beam remnant to one the further jet via another jet, reducing the overall string length.

The second meaning of CR refers to dynamical reconfigurations in colour space involving explicit exchange of momentum and colour. Dynamical reconfigurations which reduce the string length, and thus energy, may be assumed to be favoured. These dynamical reconfigurations are physical interactions in the systems, such as gluon exchanges and/or strings cutting each other up.

For e^+e^- collisions, the LC limit is a reasonable approximation as CR effects are known to be suppressed [11, 12]. Hence, many key parameters are tuned to data from

e^+e^- collisions rather than pp collisions. However in pp collisions, or more generally hadron-hadron collisions, CR effects can become much more important. This is due to the colour initial-state partons and their associated coloured beam remnants which must be taken into account. Even more significantly, due to MPIs multiple jets can reside close in phase space [13] (demonstrated by Figure 1.5), thus there is a possibility of colour reconnection between jets that can offer more favourable configurations.

2 Lund String Model

2.1 String Fundamentals

A Lund string [6] is a colour field collapsed into an idealised infinitely narrow flux tube stretched between coloured particles (typically with quark/antiquark endpoints), modelled by a 1+1 dimensional relativistic worldsheet. It is characterised by the string tension $\kappa \sim 1$ GeV/fm [6]. There are three primary string endpoint configurations to consider; a string with two endpoints (a quark and antiquark endpoint), junctions (see Section 2.5), and gluon loops (i.e. closed strings) [10].

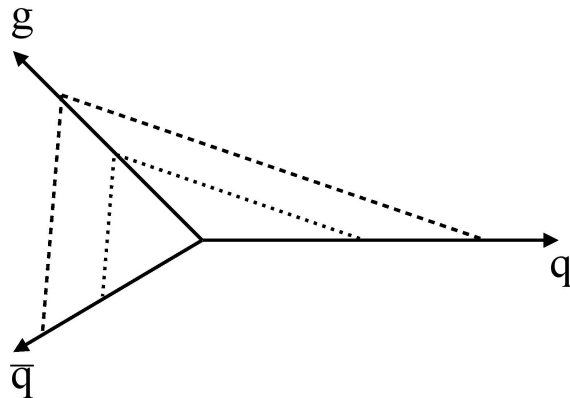


Figure 2.1. A $q\bar{q}g$ formation with the string pieces (represented by the dashed lines at two different times) stretched between the quark-antiquark pair via an intermediate gluon, forming a kink.

Consider the simplest case of a string with a quark and an antiquark endpoint, with

a number of intermediate gluons. As gluons carry both colour and anticolour charge, each gluon is colour connected to two other partons, thus they form transverse “kinks” on the string, as seen in Figure 2.1.

2.1.1 Fragmentation and Jet Production

The Lund string model supposes that when there is sufficient energy stretching a string in order to cause a string break, a quark-antiquark (or diquark-antidiquark) pair is created at the site of the break. The term “(anti)diquark”, is used to refer to two (anti)quarks. The creation of diquarks is one mechanism in which baryons are created.

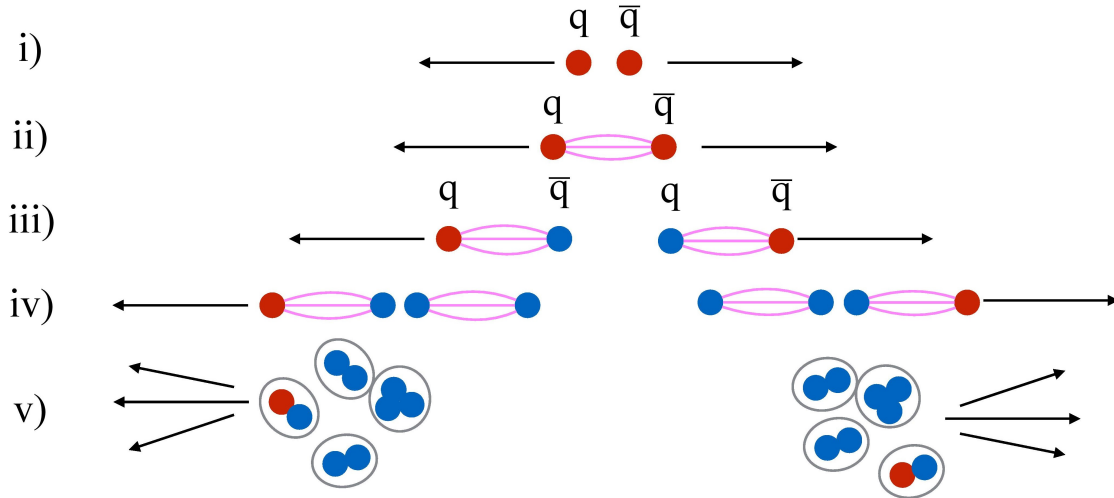


Figure 2.2. A basic schematic of hadronisation. i) Initial quarks separating with high energies, ii) a colour flux tube forming between the quarks, iii) sufficient energy in the flux tube such that another $q\bar{q}$ pair is created, iv) more $q\bar{q}$ pairs are created as the flux tubes have sufficient energy, and v) the final state consisting of colourless hadrons forming jets. Note that the colour of the quarks are for illustrative purposes and not intended to represent QCD colours, but rather simply to distinguish between the initial $q\bar{q}$ pair and the $q\bar{q}$ pairs created by string breaks.

The amount of energy required for a string break to occur is the energy needed to create at least two hadrons ($\gtrsim 1$ GeV). For example, for a system with up/down quark

endpoints, as pions are the lightest meson the minimum required energy for a break would be the mass of two pions. After a string break occurs, the remainder of the string is then spanned between each of the resulting $q\bar{q}$ pairs as can be seen in Figure 2.2 iii). This process is called string fragmentation and is described by the symmetric string fragmentation function (see Section 2.3). Fragmentation occurs at several points on the string until there's no longer sufficient energy for further creation of quark-antiquark pairs. The resulting $q\bar{q}$ pairs then form hadrons which collectively form jet structures.

The model is semi-classical, using quantum tunnelling to model the creation of quark-antiquark pairs from string breaks, but treating the endpoints classically. This limit is considered reasonable as the quantum fluctuations on the transverse component of the endpoints are of similar size to the proton radius, which is significantly smaller than the longitudinal size of the string.

When modelling fragmentation, it is useful to work in momentum space. As we are working in the semi-classical limit, we can translate the squared proper time coordinate of a given vertex to a hyperbolic coordinate, Γ , by Equation (2.2). The other useful coordinate to consider is rapidity, y , which is measured with respect to a particular axis which is conventionally labelled the z-axis. For string fragmentation, it is the axis along which the confining field is stretched (in the string CM frame). Rapidity is given by Equation (2.1), where p_z is the momentum along the assigned z-axis. It is a particularly convenient measure as it is additive under Lorentz boosts along the given axis, meaning that rapidity differences are Lorentz invariant. This allows us to formulate a Lorentz invariant approach which is desirable as the number of hadrons produced due to a given collision is then frame independent.

$$y = \frac{1}{2} \ln \left(\frac{E + p_z}{E - p_z} \right) = \frac{1}{2} \ln \left(\frac{p^+}{p^-} \right). \quad (2.1)$$

$$\Gamma = (\kappa\tau)^2 = \kappa^2(t^2 - x^2). \quad (2.2)$$

A useful measure to also consider is pseudorapidity, which unlike rapidity, it is independent of the particle mass. Pseudorapidity is a spatial coordinate that describes the angle relative to the beam axis, where θ is the angle between the 3-momentum \mathbf{p} and the positive beam axis. In the ultrarelativistic limit (i.e. moving close to the speed of light or a massless limit), we can make the approximation $\eta \approx y$.

$$\eta = \frac{1}{2} \ln \left(\frac{|\mathbf{p}| + p_z}{|\mathbf{p}| - p_z} \right) = -\ln \left(\tan \left(\frac{\theta}{2} \right) \right). \quad (2.3)$$

Another reason for the energy-momentum formulation of the Lund string model, rather than a spacetime picture formulation, is that string breaks are considered to be spacelike separated. This means that the string breaks are causally disconnected from each other, and thus can be conducted in any time order. Hence the string fragmentation process is typically modelled by string breaks occurring from each end of the string going inwards iteratively. A further consequence of the spacelike separation of vertices is a left-right symmetry in the fragmentation process, and thus the function that models string fragmentation is known as the symmetric string fragmentation function (see Section 2.3). Rapidity and the hyperbolic coordinate are key quantities when deriving the symmetric string fragmentation function [7] and will be useful to keep in mind when working in energy-momentum space below.

2.1.2 String Diagrams

In the massless relativistic limit, strings can be modelled using lightcones in Minkowski space. The simplest system to consider is the so-called yo-yo mode which represents a stable meson. In this mode, the momentum of the quark-antiquark pair is not large enough to break the string. When a string break occurs and produces a quark-antiquark pair, each such parton contributes to a different meson. This is demonstrated in Figure 2.3.

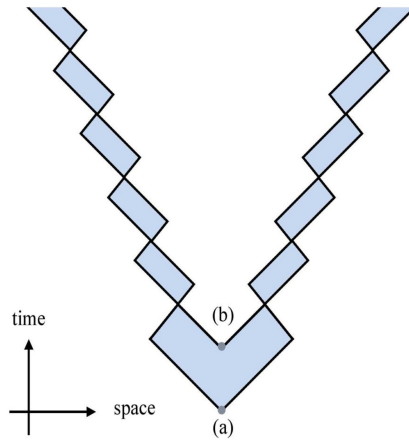


Figure 2.3. The initial state of the system, starting from vertex (a), consists of a quark-antiquark pair moving apart from one another with a string stretched between them. Then a string break occurs and vertex (b), representing the common production point of a new quark-antiquark pair, such that they each contribute towards different stable mesons represented by yo-yo modes. The areas shaded blue indicate confinement fields.

In high-energy processes, hadronisation typically involves multiple string breaks, with a causal disconnect between vertices that each create a $q\bar{q}$ pair, collectively forming a set of final-state hadrons represented by the yo-yo mode, as shown in Figure 2.4.

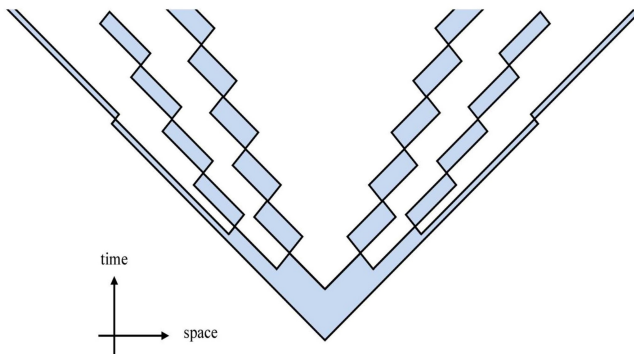


Figure 2.4. Minkowski spacetime diagram showing a $q\bar{q}$ pair moving apart with large energies, such that the field is broken in many places, causing the production of new $q\bar{q}$ pairs. The areas shaded blue indicate confinement fields.

2.2 Schwinger Mechanism

The Schwinger mechanism governs the transverse component of the fragmentation process within the Lund string framework. It was originally derived in the context of QED, and models the creation of an electron-positron pair due to the presence of a strong electric field in a vacuum [14]. It does so using quantum tunnelling provided there is sufficient energy due to the field, and the tunnelling probability is given by a Gaussian distribution.

The Lund Model assumes that the mechanism governing the equivalent process in QCD (i.e. the creation of a quark-antiquark pair due to the breaking of a string) is in the same form as the Schwinger mechanism for QED [15]. Figure 2.5 shows a comparison of the process in QED and QCD. Transferring the QED Schwinger mechanism over to QCD, the tunnelling probability for a $q\bar{q}$ pair is again given by a Gaussian, and using $m_{\perp q}^2 = m_q^2 + p_{\perp q}^2$, can be given in the form of Equation 2.4.

$$\exp\left(\frac{-\pi m_q^2}{\kappa}\right) \exp\left(\frac{-\pi p_{\perp q}^2}{\kappa}\right) = \exp\left(\frac{-\pi m_{\perp q}^2}{\kappa}\right). \quad (2.4)$$

Here κ is the string tension, $p_{\perp q}$ is the transverse momentum, m_q is an effective quark mass, and $m_{\perp q}$ is called the transverse mass. Transverse momentum and mass refers to the contribution moving in a perpendicular direction to the axis of interest, in this case the axis is the direction of the field.

The exponential term involving the quark mass results in strangeness suppression due to the strange quarks heavier mass relative to up and down quarks. Notably, unlike for electrons in the QED scenario, for the QCD Schwinger mechanism there is considerable ambiguity in the effective mass term; whether to use the constituent mass, current mass, or another value. Thus instead of directly using quark mass values, the flavour suppression factors are empirically tuned to data.

Importantly, we see that any change in the effective value of κ will translate directly to changes in strangeness suppression and transverse momentum broadening in string breaks. Specifically, an increase in string tension results in a broader p_{\perp} spectrum, and less suppression of strangeness and spontaneous diquark creation. Thus using an effective increased string tension, κ_{eff} , results in baryon and strangeness enhancement. This mechanism is a strong motivator for increasing the string tension via close packing in order to give a rise in strangeness ratios explored in Section 3.

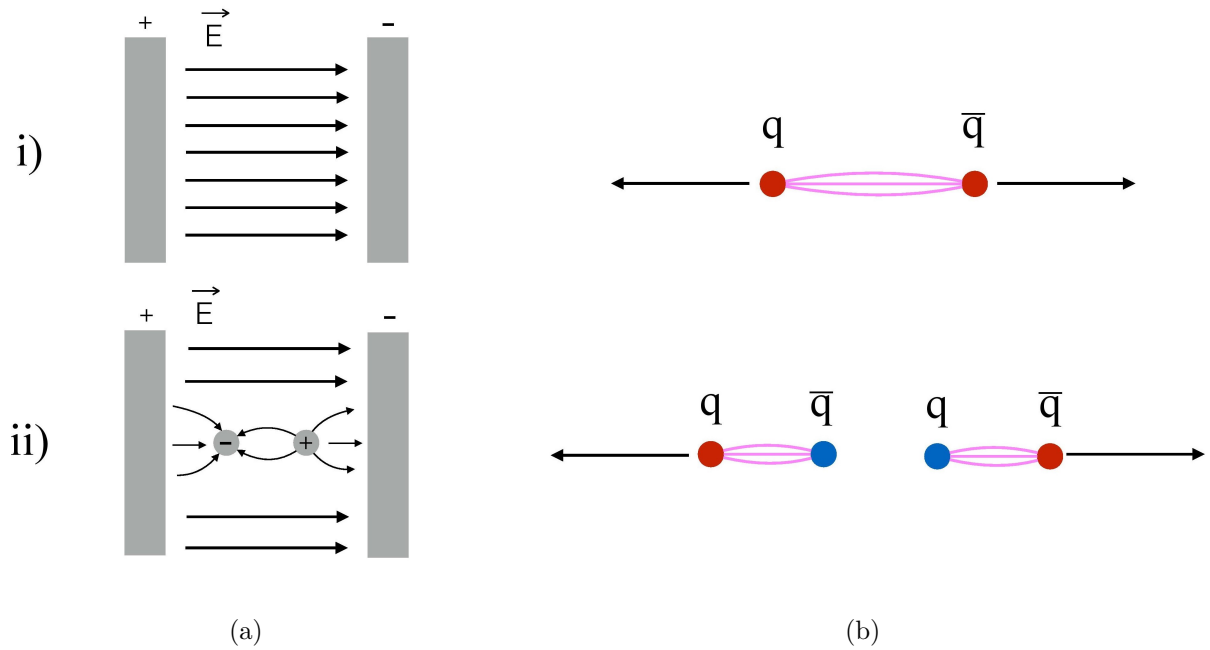


Figure 2.5. A comparison between the Schwinger mechanism in QED (a) and QCD (b). i) shows the the strong field and ii) shows the pair creation due to the strong field. Note that the colour of the quarks are for illustrative purposes and not intended to represent QCD colours, but rather simply to distinguish between the initial $q\bar{q}$ pair and the $q\bar{q}$ pair created by the string break.

2.3 Symmetric Fragmentation Function

The fragmentation function is the probability distribution that governs the longitudinal component of the fragmentation process; for a hadron with transverse mass m_{\perp} , it specifies the probability that the resultant hadron will have a given fraction z of the total energy, or conversely the probability that the string will retain a given fraction $(1 - z)$ of the total energy. Due to the causal disconnect of string breaks in the Lund model, the fragmentation function has been formulated in a left-right symmetric manner.

The symmetric fragmentation function used in the Lund String Model is given by Equation (2.5) [7] with free parameters a and b , and normalisation constant N such that the distribution over all z it is normalised to unity. Large values of a suppresses the $z \rightarrow 1$ limit. In other words, it suppresses the limit in which the hadron takes

all the momentum. Increasing the parameter b increases the peak amplitude of the Gaussian component. The symmetric fragmentation function is given by

$$f(z) = N \frac{1}{z} (1-z)^a \exp\left(\frac{-bm_{\perp}^2}{z}\right). \quad (2.5)$$

Further indepth examination into probability distributions governing string topologies is outside the scope of this review, however for further understanding see [7] and [16].

2.4 Lambda measure

It is useful when discussing strings to talk about the “string length”. A so-called longer string requires a greater amount of energy than a “shorter” one. Rather than using a spatial measure of length, which is a relative quantity, a Lorentz-invariant measure called the lambda measure is used instead. It is a measure of the energy density per unit length of the string.

The lambda measure for a quark-antiquark system (with any number of intermediate gluon kinks) is given by Equation (2.6), and indicates a logarithmic growth in string length.

$$\lambda^{q\bar{q}} = \ln\left(1 + \frac{m^2}{2m_0^2}\right). \quad (2.6)$$

where m is the dipole mass, and m_0 is of order Λ_{QCD} [12, 17].

2.5 Junctions

Junctions topologies are a beyond-LC phenomenon where three strings meet at the one vertex [17], and contribute to baryon production. For this discussion, we will look at the simplest junction topology; a Y-shaped configuration between qqq or $\bar{q}\bar{q}\bar{q}$, as seen in Figure 2.6.

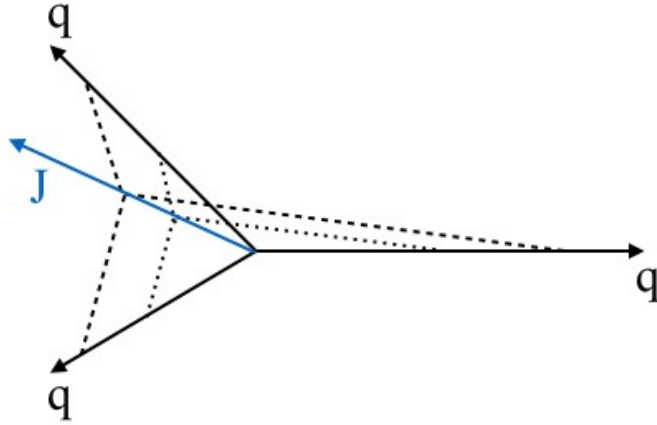


Figure 2.6. Junction system, involving a Y-shaped string topology between three quarks.

Figure 2.7 shows the formation of junctions due to CR, showing the reconfiguration of three $q\bar{q}$ pairs into a junction and antijunction.

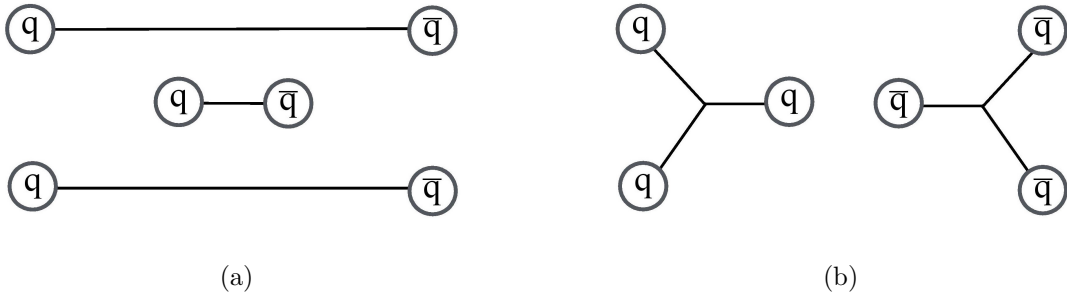


Figure 2.7. (a) Strings spanning $q\bar{q}$ pairs. (b) A reconfiguration of the strings instead forming a junction and corresponding antijunction. This junction configuration can only form if the overall qqq (and thus also $\bar{q}\bar{q}\bar{q}$) are in an overall colour singlet state.

The string-fragmentation mechanism for junctions can be formulated as an extension (albeit a complicated one) of the model for a simple string stretched between a $q\bar{q}$ pair [17]. The inclusion of junction fragmentation results in a higher number of baryonic final states as the baryon number of the junction topology is preserved by the fragmentation process, as seen in Figure 2.8. It should be noted that though the total number of baryonic final states increases (i.e. $\sum |B|$ increases where B is the baryon

number), the total baryon number ($\sum B$) conservation is not violated as CR ensures an equal number of junctions and antijunctions (see Figure 2.7).

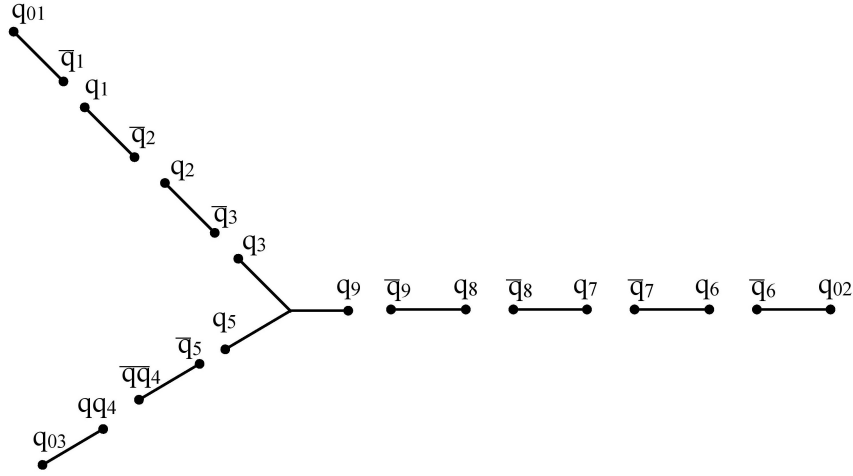


Figure 2.8. Hadronisation of junction topology, with arbitrary labelling of quarks. The qq_4q_{03} and $\bar{q}\bar{q}_4\bar{q}_5$ hadrons come from spontaneous baryon-antibaryon pair production, and the original baryon number is carried by the $q_3q_5q_9$ hadron. The remainder of hadrons produced are mesons.

The effect of allowing for junction topologies can be seen in Figure 2.9, which shows the ratio of Λ baryons to K_S^0 mesons versus rapidity. Importantly, Λ baryons and K_S^0 mesons have the same strangeness, thus the data gives a measure of baryon production relative to meson production for equal strangeness. Modes 0, 2 and 3 [12] include CR with junctions, whereas Monash 2013 [4] tune does not. However it must be noted that though the inclusion of junctions can predict the baryon enhancement, it cannot explain the strangeness enhancement seen in Figure 3.1.

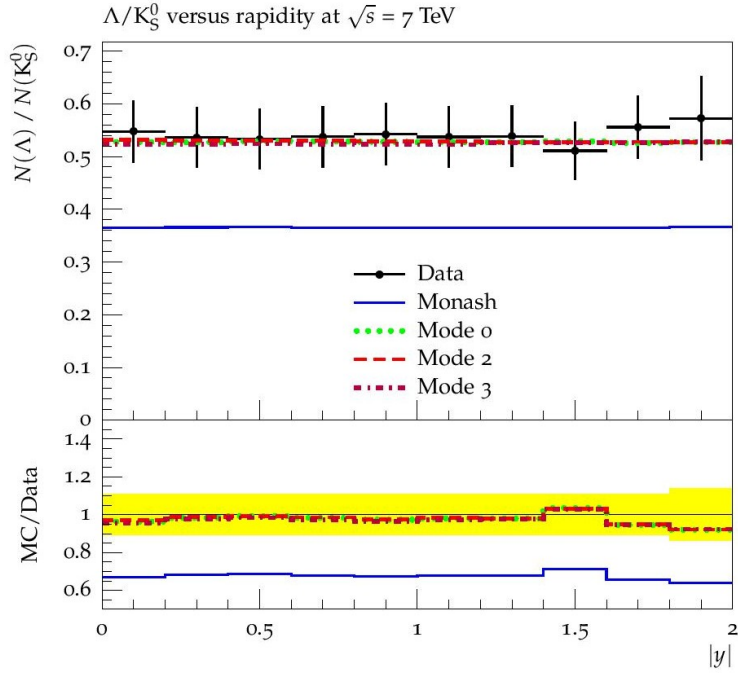


Figure 2.9. The ratio of Λ/K_S^0 with respect to rapidity, plotted with the Rivet framework [18]. The observables are from the CMS collaboration, and are non single diffractive (NSD) events. All PYTHIA simulations have no p_\perp cuts but do have a lifetime cut-off of $\tau_{max} = 10$ mm/c. The Modes 0, 2 and 3 include junctions and CR effects [12].

3 Close Packing

One shortcoming of the Lund string model is its predictions of constant strangeness ratios in pp collisions. Figure 3.1 plots results from the ALICE collaboration at the LHC, showing the ratio of yields of strange hadrons relative to pions ($\pi^+ + \pi^-$). The data shows a rise in strangeness with respect to the overall number of charged particles in the event, known as the “charged particle multiplicity”. In particular there is a rise in multistrange hadrons. Currently the default PYTHIA tune predicts a constant ratio of yields rather than a rise as seen in the ALICE data.

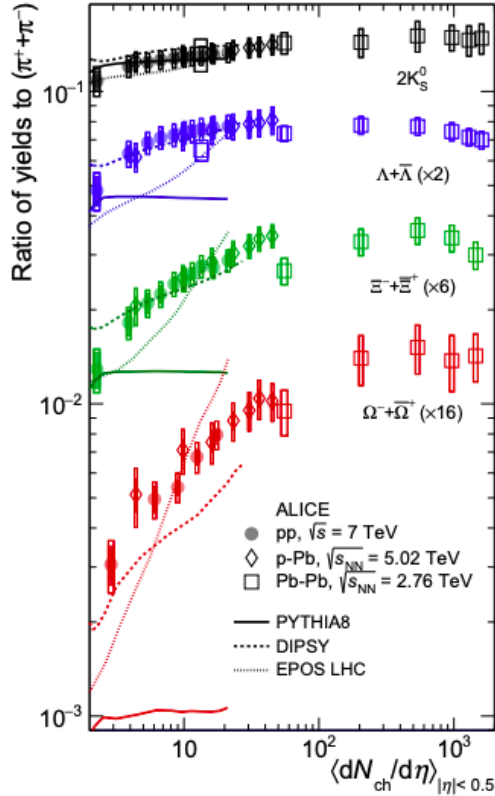


Figure 3.1. Experimental results from the ALICE collaboration [1] showing the increase in strangeness ratios with multiplicity, with model predictions from PYTHIA [3], DIPSY [19] and EPOS [20]. The p_{\perp} -integrated ratio of yields to $(\pi^{+} + \pi^{-})$ are measured in $|y| < 0.5$, as a function of $\langle dN_{ch}/d\eta \rangle_{|\eta| < 0.5}$.

As discussed in Section 2.2, due to the form the Schwinger mechanism takes (see Equation (2.4)), an increased string tension results in reduced strangeness suppression. Thus in order to create a model that can describe the ALICE data, we introduce a mechanism that increases string tension with charged multiplicity: close packing. This mechanism was introduced in an earlier study [5] in the context of the thermodynamical model, and here we generalise the model implementation to the Schwinger-type string breaks.

Close packing is the collective effect of multiple strings contributing to an effective string tension which is dependent on number of strings in the near vicinity. This is a similar mechanism of altering the string tension as used by the Rope Model [21]. How-

ever, in the Rope Model, a “rope” is a structure of strings acting coherently where string breaks occur in a particular order due to the rope construction. Contrastingly, close packing instead treats the surrounding strings as an overall background contribution to the effective string tension, with no modified ordering of fragmentation.

When measuring the number of strings that contribute to the effective string tension in the close packing model, surrounding strings are counted if they have rapidity overlap with the hadron resulting from the fragmented string. The rapidity is measured with respect to the beam axis. In pp collisions this is a reasonable measure as protons are comprised of coloured partons, hence due to beam remnants, the majority of the strings are expected to be orientated along the beam axis.

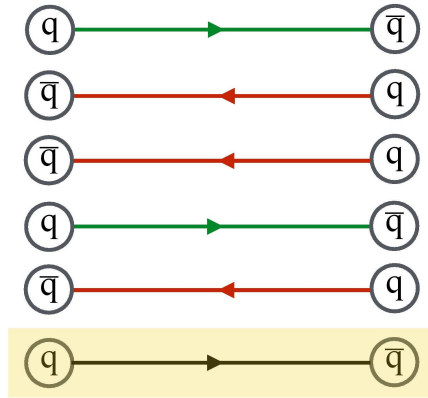


Figure 3.2. A simple illustration of a collective of strings, each spanned between a quark and antiquark. In this example, we consider the number of surrounding strings for the yellow highlighted string system. For the flux-blind model, the overall total number of background strings is counted, which in this example is five strings. For the flux-sensitive model, the direction of colour flow is indicated by the arrows. There are two parallel strings (shown by the green strings) and three antiparallel strings (shown by the red strings).

The formulation we implemented in PYTHIA is given by Equation (3.1). In this formulation, κ_0 is the initial vacuum string tension, p is the number of strings with “parallel flux”, q is the number of strings with “antiparallel flux”, and k_P and k_A are the weighting of the contributions of parallel and antiparallel strings respectively. The term flux is defined by the colour flow of the string, whether we are going from triplet

to antitriplet or vice versa. Figure 3.2 gives a simple schematic of what is meant by flux sensitivity.

$$\kappa_{eff} = \left(1 + k_P \left(\frac{p + \frac{k_A}{k_P} q}{1 + p_{\perp Had}^2 / p_{\perp 0}^2} \right) \right)^{2r} \kappa_0. \quad (3.1)$$

The form provided by Equation (3.1) allows for the altering of the strength of the background strings on an effective string tension, as well as adjustment of the the degree of flux sensitivity. This can be done via the altering of k_P (`ClosePacking:tension`) and k_A/k_P (`ClosePacking:tensionRatio`). Alternatively, rather than linearly scaling the effective strength of the background strings (via changing k_P and k_A , a non-linear power relation can instead be used, where the parameter r is tuned to data.

We expect this contribution of surrounding strings to be suppressed should the fragmenting string have a high p_{\perp} . This is as a string with high p_{\perp} will be further away from the overall collective of strings, and thus less sensitive to the background contributions from the surrounding strings. This effect is implemented via the $p_{\perp Had}$ term in the denominator of Equation (3.1), and is scaled by the term $p_{\perp 0}$.

It is useful to consider the limits of large and vanishing $p_{\perp Had}$ to make sense of this relation. At large $p_{\perp Had}$, the expected contribution from the collective of strings would be very little, and is reflected by the limit of Equation (3.1), where κ_{eff} approaches κ_0 . Conversely, at $p_{\perp Had} = 0$, the contribution from the collective of near strings would be maximised, and thus as the denominator reduces to 1, the effective string tension becomes only dependent on the number of background strings.

Within this formulation, there are two special cases that can be considered; Casimir scaling and a flux-blind model. The flux-blind model assumes that the flux direction of a string has no impact on the strength of its contribution to the overall background. In other words, a flux-insensitive model treats each string on equal footing and is implemented by setting `ClosePacking:tensionRatio` to unity.

In order to determine the strength of the contributions of the opposing and agreeing flux strings, one possible motivation for the parameter choices is Casimir scaling. Casimir scaling is derived from group theory and when applied to SU(3) static potentials, it provides the scaling of the string tension resulting from overlapping strings [22]. For the model to follow exact Casimir scaling, $k_P = 0.25$, $k_A = 0.125$ and $r = 0.5$. This

4 Implementation in PYTHIA

To observe the effects of close packing of Lund Strings, the model is implemented in PYTHIA [2, 3], a Monte-Carlo event generator developed in C++. The relevant parameters in the model and their mathematical representations are given by Table 1.

Table 1: PYTHIA close packing parameters and their corresponding mathematical notation as used in section 3.

PYTHIA Parameters	Mathematical symbol
ClosePacking:allow	-
ClosePacking:expNSP	r
ClosePacking:PT0	$p_{\perp 0}$
ClosePacking:tension	k_P
ClosePacking:tensionRatio	$\frac{k_A}{k_P}$
ClosePacking:facQQ	f_{QQ}

4.1 Probabilities

A set of parameters impacted by a changing string tension are `probStoUD`, `probSQtoQQ`, `probQQ1toQQ0` and `probQQtoQ`, which belong to the `StringFlav` class in PYTHIA. These probabilities determine how likely a quark or diquark with given flavours or spin are produced. It should be noted that the up and down quarks are treated on the same footing with equal probabilities.

`StringFlav:probStoUD` is the ratio of the probability of creating a strange quark via a string break relative to the probability of creating an up/down quark. In the default Monash 2013 PYTHIA tune, it is given as 0.217, which was tuned to the K/π ratio (and other related quantities [4]) in e^+e^- collisions. However as seen in Figure 3.1, this ratio no longer is sufficient in pp collisions. According to the Gaussian form of the Schwinger mechanism in Equation (2.4), the probability ratio thus takes the form:

$$P(s : u/d) = \frac{P(m_s^2)}{P(m_{u/d}^2)} = \frac{\exp\left(-\frac{\pi m_s^2}{\kappa_0}\right)}{\exp\left(-\frac{\pi m_{u/d}^2}{\kappa_0}\right)}. \quad (4.1)$$

Likewise, the probability with an effective string tension is given by:

$$P'(s : u/d) = \exp\left(-\frac{\pi(m_s^2 - m_{u/d}^2)}{\kappa_{eff}}\right). \quad (4.2)$$

The Gaussian form allows for a simple relationship between the probabilities with κ_0 and κ_{eff} , demonstrated by Equation (4.3).

$$P'(s : u/d) = \exp\left(-\frac{\pi(m_s^2 - m_{u/d}^2)}{\kappa_0} \frac{\kappa_0}{\kappa_{eff}}\right) = P(s : u/d)^{\frac{\kappa_0}{\kappa_{eff}}}. \quad (4.3)$$

Alongside `probStoUD`, the probabilities `probSQtoQQ` and `probQQ1toQQ0` also take the same form of modification as shown in Equation (4.3). Note that κ_{eff} is proportional to κ_0 , as seen in Equations (3.1), thus the ratio κ_0/κ_{eff} takes a form independent of κ_0 .

`StringFlav:ProbQQtoQ` however takes a more complex form as it is a global probability. `ProbQQtoQ` is described by Equation (4.4) [23]. The variable α is dependent on `probStoUD`, `probSQtoQQ` and `probQQ1toQQ0`, the full form which can be seen in Appendix B.

$$P(qq : q) = \alpha \frac{\mathcal{P}_{ud0}}{\mathcal{P}_u}. \quad (4.4)$$

Assuming we do not know how the probability $\mathcal{P}_{ud0}/\mathcal{P}_u$ scales with an effective string tension, we instead use a simple parametrisation given in Equations (4.5) and (4.6). As $f_{QQ} \rightarrow 1$, $\mathcal{P}_{ud0}/\mathcal{P}_u$ scales as per `probStoUD`, whereas when $f_{QQ} \rightarrow 0$, an effective string tension does not alter $\mathcal{P}_{ud0}/\mathcal{P}_u$.

$$R_\kappa^{QQ} = 1 + f_{QQ}^2 \left(\frac{\kappa_{eff}}{\kappa_0} - 1\right). \quad (4.5)$$

$$P'(qq : q) = \tilde{\alpha} \left(\frac{P(qq : q)}{\alpha}\right)^{1/R_\kappa^{QQ}}. \quad (4.6)$$

The variable $\tilde{\alpha}$ is calculated in the same manner as α , except with the effective string tension taken into account. See Appendix B for a full derivation and explanation of these quantities and relations.

4.2 p_{\perp} Distribution

The altered effective string tension also affects the p_{\perp} spectrum of the produced hadrons. The width of the p_{\perp} spectrum is given by σ^2 , where σ is stored in PYTHIA as `StringPT:sigma`. Using the tunneling probability given by the Schwinger mechanism, equation (2.4), the average p_{\perp} value is given in the form:

$$\langle p_{\perp}^2 \rangle = \frac{\pi}{\kappa_0} \int_0^{\infty} p_{\perp}^2 \exp\left(\frac{-\pi p_{\perp}^2}{\kappa_0}\right) dp_{\perp}^2 = \frac{\kappa_0}{\pi}. \quad (4.7)$$

This allows for a simple relation between `StringPT:sigma` with and without an effective string tension. Equation (4.8) shows that `StringPT:sigma` scales with a multiplicative factor of $\sqrt{\kappa_{eff}/\kappa_0}$.

$$\sigma'^2 = \frac{\kappa_{eff}}{\pi} = \frac{\kappa_0}{\pi} \frac{\kappa_{eff}}{\kappa_0} = \sigma^2 \frac{\kappa_{eff}}{\kappa_0}. \quad (4.8)$$

4.3 PYTHIA Functions

In implementing close packing in PYTHIA, the variable R_{κ} (`kappaRatio`) is calculated in the `StringFragmentation` function `kappaEffectiveRatio`, which returns the effective strength of the collective of strings, and is defined by Equation (4.9). In this function, a temporary test hadron is created to approximately determine where we are in rapidity space, and hence is used to determine the local density of background strings. Prior to creating a new quark-antiquark pair due to a string break, the relevant probabilities are reinitialised in the function `StringFlav::reinit`.

$$\kappa_{eff} = (R_{\kappa})^{2r} \kappa_0. \quad (4.9)$$

In order to count the number of near string pieces, rapidity overlap is used. The rapidities of the collective of strings are recorded in the `HadronLevel` function `rapidityPairs`, which stores the rapidities of the partonic endpoints of each segment of string as a rapidity pair. The rapidity pairs are ordered such that the direction of the colour flow goes from the first to the second parton in the pair. For example, if we had the case of a simple $q\bar{q}$ pair with a single intermediate gluon, two rapidity pairs would be recorded; $\{y_q, y_g\}$ and $\{y_g, y_{\bar{q}}\}$.

A similar treatment is given to junction systems, however at this stage in the implementation, due to the time constraints of the project, the junction rapidity pair calculations neglect gluons. For a more complete picture, gluon kinks should also be considered in the scope of junctions. Figure 4.1 demonstrates the colour flow of two example junction systems. The full code can be seen in Appendix C.

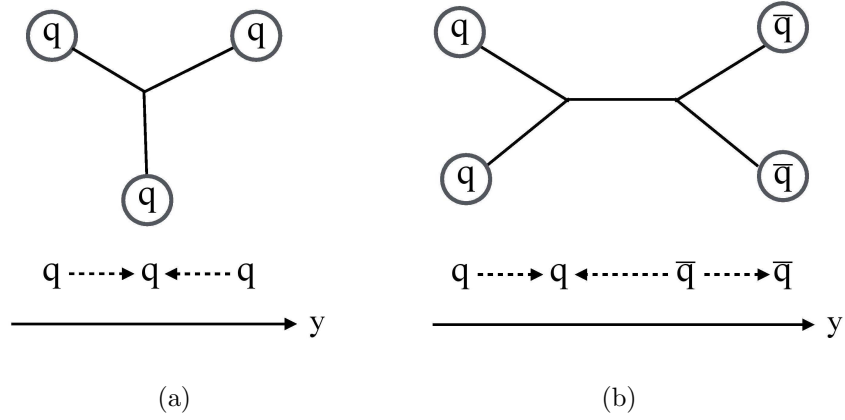


Figure 4.1. Ordered in rapidity with respect to the z -axis, the colour flow direction, as indicated by the dashed arrows, of (a) A standard Y-shaped qqq junction system. (b) A double junction system.

5 Results

In this section, we firstly retrace to the motivation for this study; the data from the ALICE collaboration showing the strangeness ratios as a function of charged multiplicity. We present both the existing models in PYTHIA and the implementation of our close packing model. Then we include some validation distributions from the CMS collaboration, to ensure that our close packing model and tuning to the ALICE data does not compromise the ability to describe other relevant distributions. Finally we address shortcomings of the model and proposed areas in which further examination is warranted.

5.1 ALICE Strangeness Data

Before examining the consequences of close packing, we compare the existing implementations in PYTHIA; the default PYTHIA Monash 2013 tune [4], the QCD CR model [12], and the Rope Model [21]. The specific mode used for QCD CR here is Mode 2, which requires a causal connection between all dipoles involved in a given reconnection (for details, see [12]). The predictions of these models are shown in Figure 5.1. For all PYTHIA simulations, 1,000,000 events were generated.

The events simulated in PYTHIA, as well as those from the ALICE data, are inelastic pp collisions at $\sqrt{s} = 7$ TeV and are limited to those having at minimum one charged particle within the pseudorapidity interval of $|\eta| < 1$. The yields of $K_S^0, \Lambda + \bar{\Lambda}, \Xi^- + \bar{\Xi}^+, \Omega^- + \bar{\Omega}^+, p + \bar{p}$ and $\pi^+ + \pi^-$ (which in the following will be denoted simply as $K_S^0, \Lambda, \Xi, \Omega, p$ and π) include only so-called “primary particles”, with $|y| < 0.5$. Primary particles are a specific set of hadrons and leptons detected in collision events (the full list of included particle types can be found in Appendix D) are determined by ensuring none of the ancestor particles are also primary. In other words, decay products of a given primary particle are not also counted as primary.

The particles K_S^0, Λ, Ξ , and Ω are examined in particular as they are all weakly decaying and long-lived, thus easier to detect. The particle K_S^0 is used as it is the lightest single-strange meson. Similarly, the Λ, Ξ and Ω are the lightest single-, double- and triple-strange baryons respectively.

The multiplicity dependence is studied according to event classes, which are determined by examining the charged particle multiplicity in the forward detectors, spanning the pseudorapidities $2.8 < \eta < 5.1$ and $-3.7 < \eta < -1.7$. In ALICE parlance, this is called the “V0M” multiplicity. The event classes are determined using centrality bins which decrease progressively with the average midrapidity charged multiplicity, $\langle dN_{ch}/d\eta \rangle_{|\eta| < 0.5}$. For further clarification, see Appendix D.

As can be seen in Figure 5.1, the Monash tune predicts a constant strangeness ratio (as per Figure 3.1 provided by ALICE). CR only results in an increase in baryon production with respect to charged particle multiplicity, however it is not significant enough to describe the data, nor can it account for the rise seen in the K_S/π ratio, meaning it lacks strangeness enhancement. The Rope model does show behaviour of strangeness enhancement with increasing charged particle multiplicity, albeit the Λ/π ratio is overestimated significantly, particularly at high multiplicities. We note that the Rope model is also rather computationally expensive, a point we shall return to below.

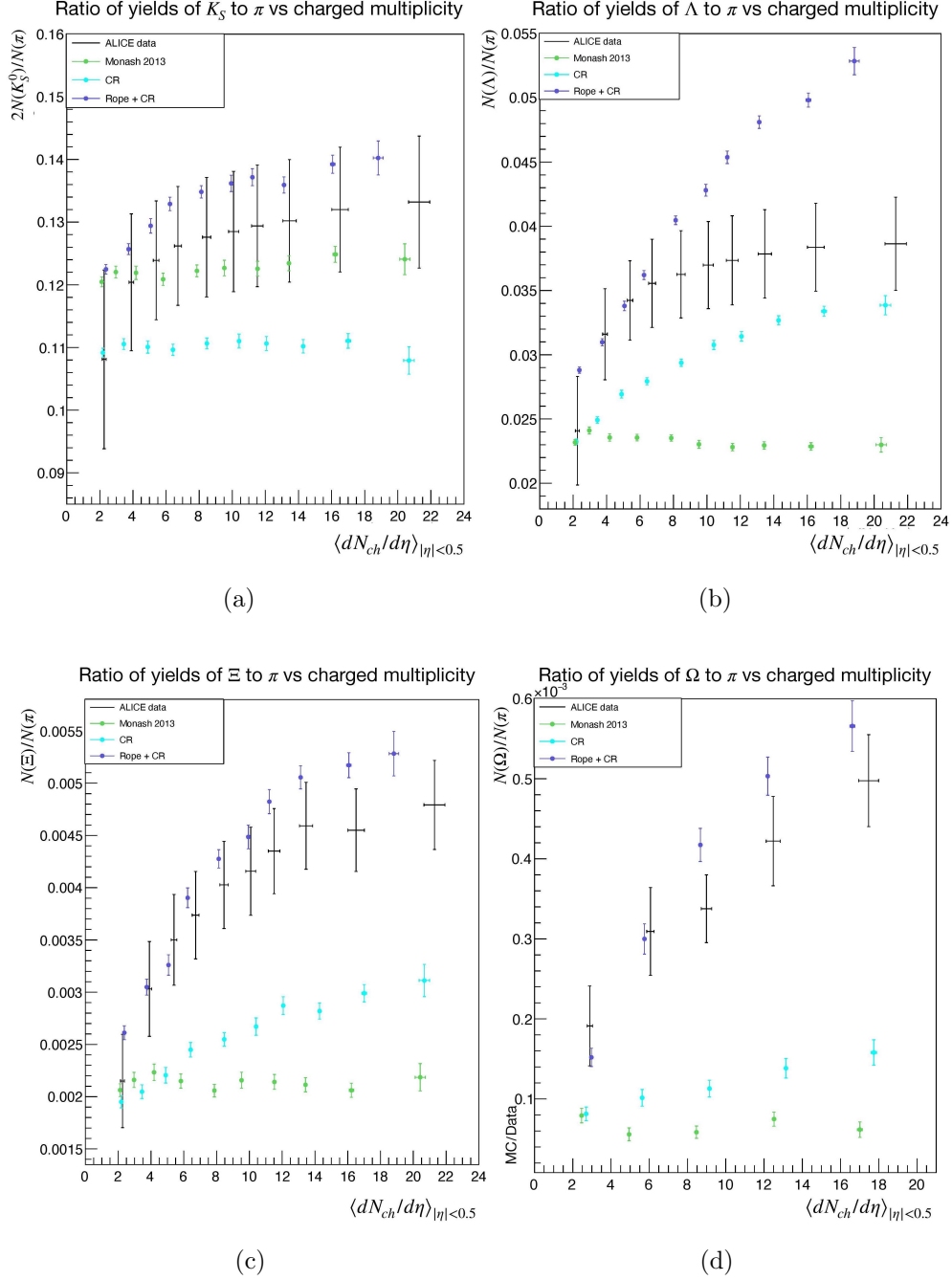


Figure 5.1. Comparison of the ALICE data to existing PYTHIA implementations, including PYTHIA’s default tune (the Monash 2013 tune [4]), the QCD CR model (Mode 2) [12], and the Rope model [21, 23]. Shown are the ratio of strange hadrons to $(\pi^+ + \pi^-)$ in $|y| < 0.5$ vs the average midrapidity charged multiplicity, $\langle dN_{ch}/d\eta \rangle_{|\eta|<0.5}$. The events simulated are inelastic pp collisions at $\sqrt{s} = 7$ TeV, with no p_\perp or lifetime cuts, and counting only primary particles.

Figure 5.2 displays the implementation of CR in combination with four different close packing model variations; with flux-sensitivity on or off, and with either linear or non-linear scaling. The parameter `ClosePacking:tensionRatio` is determined by the model variation, where the flux-insensitive model uses `tensionRatio = 1` and the flux-sensitive model uses `tensionRatio = 0.5` (corresponding to Casimir scaling).

When using non-linear scaling, `ClosePacking:tension` is either fixed to 0.25 for a flux-sensitive model (for Casimir scaling), or to 1 for the flux-blind model. `ClosePacking:expNSP` is then tuned to the overall amount of strangeness enhancement required. Contrastingly, when using linear scaling, `ClosePacking:expNSP` is fixed to 0.5 and `ClosePacking:tension` is instead the parameter tuned to the degree of strangeness enhancement required.

The parameter `ClosePacking:facQQ` controls how much the effective string tension affects baryon production. From varying this parameter, we observed that a higher f_{QQ} value resulted in an increase in low strangeness baryon production, whereas $f_{QQ} \rightarrow 0$ results in a lower overall baryon production rate however more of those baryons had multistrange compositions. The parameter `ClosePacking:PT0` controls the strength of the p_{\perp} suppression in calculating κ_{eff} . We expect `ClosePacking:PT0` values to range from approximately 0.4 to 2, such that it is of order of the average p_{\perp} of hadrons created in such events. The p_{\perp} dependence was not investigated in detail in this study, and $p_{\perp 0}$ was fixed to 0.6, which should be reasonably representative of the transition between remnant and jet fragmentation.

Figure 5.2 shows that the close packing model describes the non-trivial rise in strangeness with charged multiplicity fairly well. However, we are yet to tune the model such that it can accurately describe the saturation of strangeness enhancement the ALICE data shows at high multiplicities. It is worth noting that in order for close packing to produce sufficient strange baryon production rates, the ratio of kaons to pions is overpredicted. Comparing Figures 5.1 and 5.2, the close packing model appears to be able to describe the ALICE data at least as well as the Rope model, perhaps even slightly better. The full list of parameters used for each model are given in Appendix A. Notably, for the flux-sensitive models, the deviation from exact Casimir scaling is approximately a 40% decrease overall. Such variance from exact Casimir scaling might be explained by the fact that our system is not comprised of nicely aligned static QCD charges (which is how Casimir scaling is determined), but rather a dynamic collection of strings.

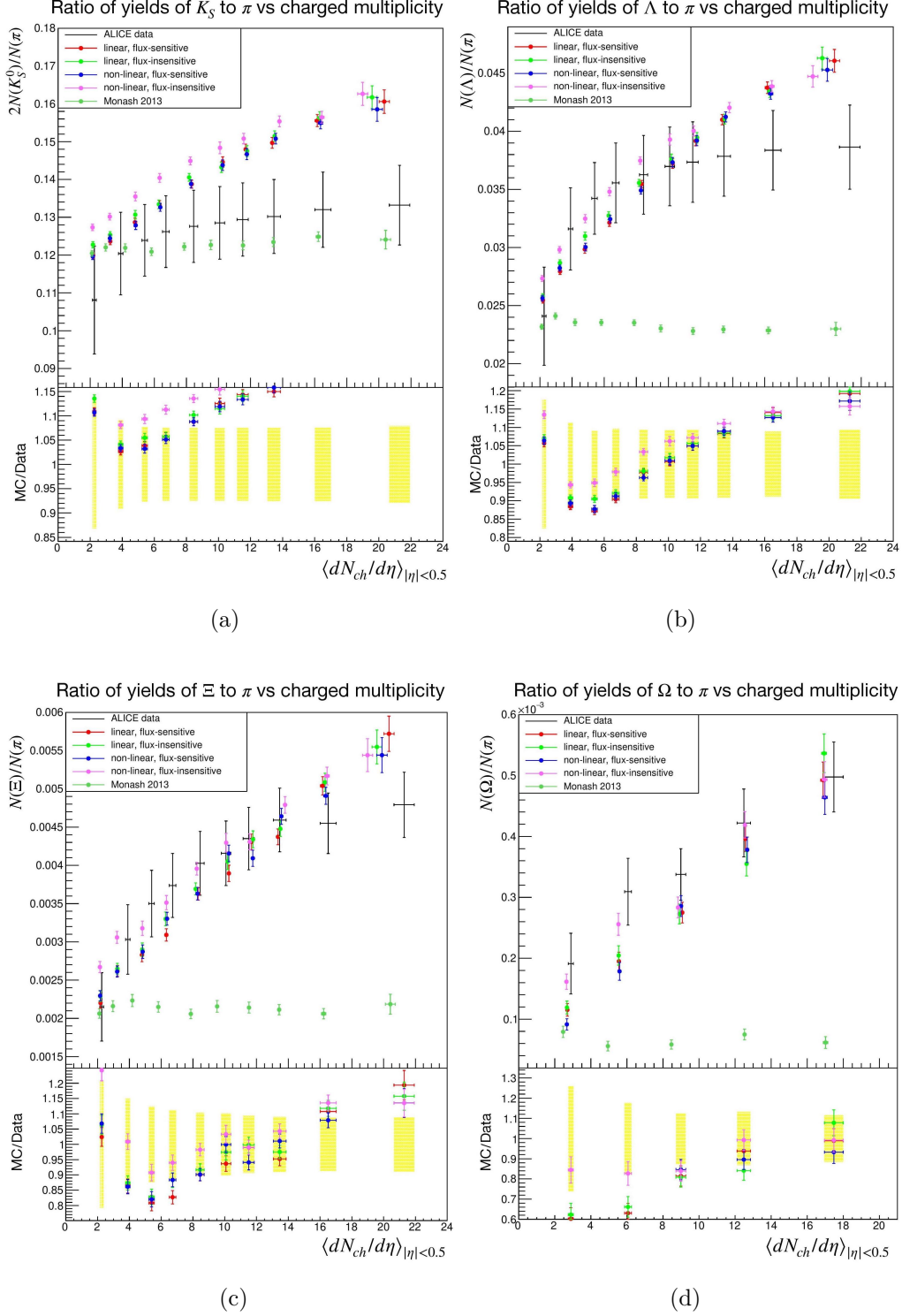


Figure 5.2. Close packing model variations alongside the default PYTHIA tune and the ALICE data. Shown are the ratio of yields of strange hadrons to pions ($\pi^+ + \pi^-$) measured in $|y| < 0.5$ with respect to $\langle dN_{ch}/d\eta \rangle_{|\eta|<0.5}$ for inelastic pp collisions at $\sqrt{s} = 7$ TeV. No lifetime cut made or p_{\perp} cuts applied to the event generation. 31

From these results alone however, we cannot split the degeneracy between the four variations of our model. In order to do so, comparison to other data would need to be carried out, particularly examination of differential distributions such as p_{\perp} spectra. There are also other strange hadron distributions that would be useful to examine, such as K^* and ϕ [24]. Such distributions have not been looked at thus far due to the time constraints of the project, however should be targeted further in future works.

5.2 Model Efficiency

Alongside the promising results outlined above, another advantage of close packing is its runtime. Figure 5.3 displays the runtimes with respect to charged multiplicity of the default PYTHIA tune, the Rope model with CR, and our close packing model with CR (in particular, the linearly-scaled flux-sensitive variation of the close packing model). Notably our close packing model is far less computationally expensive than the Rope model, while seemingly still competitive in describing the ALICE data of the strangeness ratios. The greater runtime of the Rope model is chiefly due to its use of explicit spacetime evolutions in timesteps, significantly increasing the complexity of that implementation.

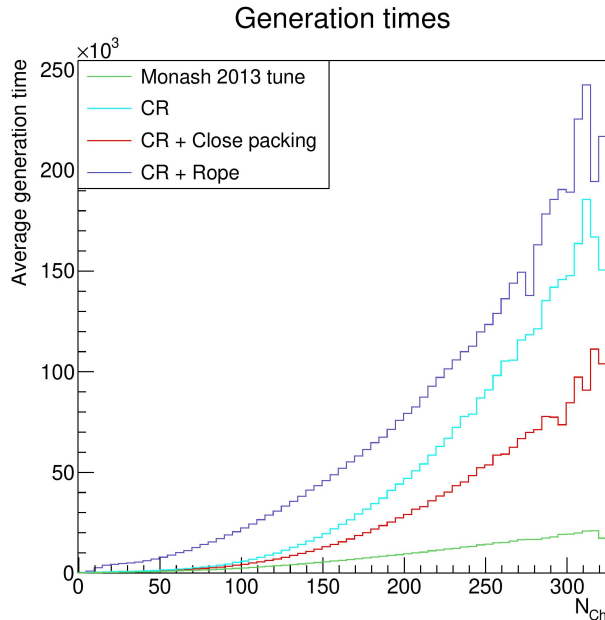


Figure 5.3. The average generation time per event of each respective model with respect to the charged multiplicity of primary particles. No p_{\perp} or rapidity cuts were made.

Figure 5.3 also shows that particularly at high multiplicities, close packing in conjunction with CR is faster than CR alone. This is due to the parameter `MultiPartonInteractions:pT0Ref` being greater in the close packing tune (specifically 2.2 instead of the CR Mode 2 value of 2.15). Increasing this parameter means that there are less MPIs and thus less CR effects, therefore resulting in a reduced runtime. This demonstrates that the implementation of close packing contributes very little to the runtime overall, but rather it is predominantly dependent on CR.

5.3 CMS Observables

The event structures are a complicated combination of many physics effects, therefore multiple sets of data need to be examined so that agreement with one set does not sacrifice agreement with another. Here we use the CMS data [25–27] as a control mechanism to ensure fitting to the ALICE strangeness data doesn’t sacrifice agreement with these CMS observables. These in particular are used as they measure global aspects of the charged-particle modelling, and are also used in the QCD CR paper, thus allowing for a direct comparison.

The observables from the CMS collaboration are particularly sensitive to the CR tuning parameters. With the implementation of CR, specifically Mode 2, PYTHIA has been able to describe the Λ/K_S data whilst remaining consistent with data from LEP. CR has three main tuning parameters; `ColourReconnection:timeDilationPar`, `ColourReconnection:junctionCorrection`, and `MultiPartonInteractions:pT0Ref`. The parameter `ColourReconnection:timeDilationPar` is tuned to the $\langle p_{\perp} \rangle$ vs N_{ch} distribution and controls the strength of the CR effect. `ColourReconnection:junctionCorrection` is the ratio m_{0j}/m_0 , a multiplicative factor to the string-length measure for junction systems, thus altering the probability of junction reconnections, and is tuned to the Λ/K_S^0 ratio. Lastly the `MultiPartonInteractions:pT0Ref` parameter is the lower regularisation scale of the MPI framework and is tuned to the $d\langle N_{ch} \rangle/d\eta$ distribution.

The CMS observables along with the PYTHIA simulations are shown in Figure 5.4, 5.5, and 5.6. All events involved are non-single diffractive (NSD), with Figures 5.4 and 5.5 at 7 TeV and Figure 5.6 at 900 GeV respectively. From these results, we can see that close packing is able to describe most of the CMS data consistently. However as seen in subfigures (c) and (d) in Figures 5.5 and 5.6, the close packing simulations are not yet able to fully describe the ratio of yields of strange hadrons with respect

to transverse momentum. In the scope of this project, we have not placed a focus on p_{\perp} distributions and the effects of close packing on momentum, however it would be useful to look at differential p_{\perp} distributions in order to further tune the model and aim to describe this data. Again, we note that these distributions also do not provide any indication to split the degeneracy between the variations of the close packing model.

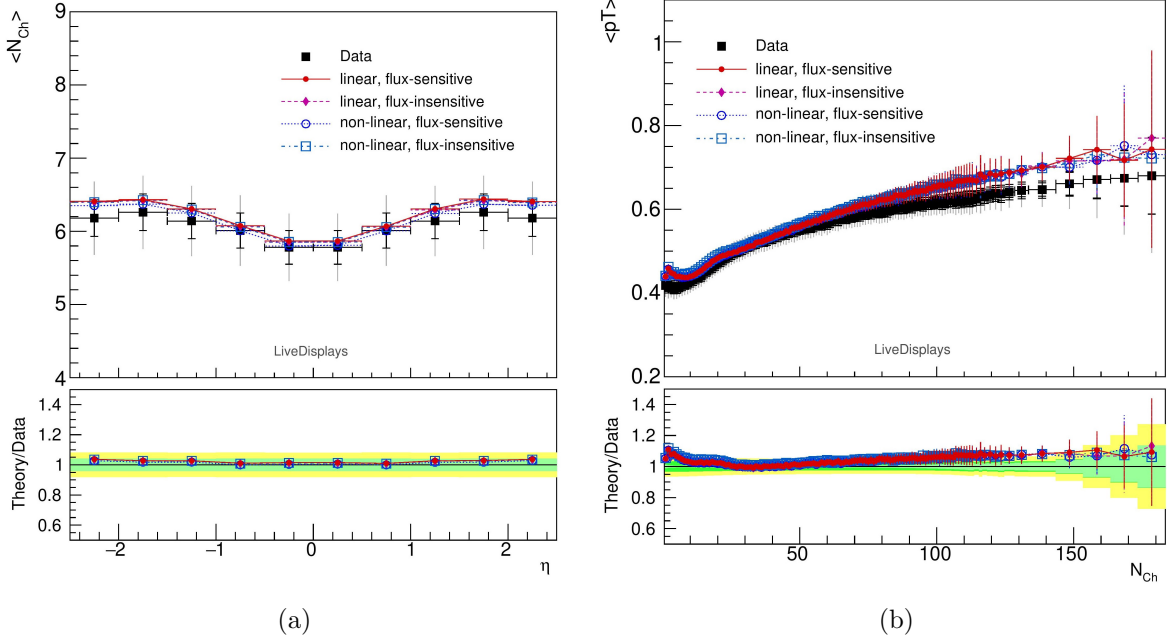


Figure 5.4. (a) The average charged multiplicity with respect to pseudorapidity [26]. (b) The the average transverse momentum with respect to the charged multiplicity within the range $|y| < 2.4$ [27]. Events are non-single diffractive at $\sqrt{s} = 7$ TeV. The models shown here are the different variations of the close packing model. A lifetime cut of $\tau_{max} = 10$ mm/c is made and no p_{\perp} cuts are applied to final state particles.

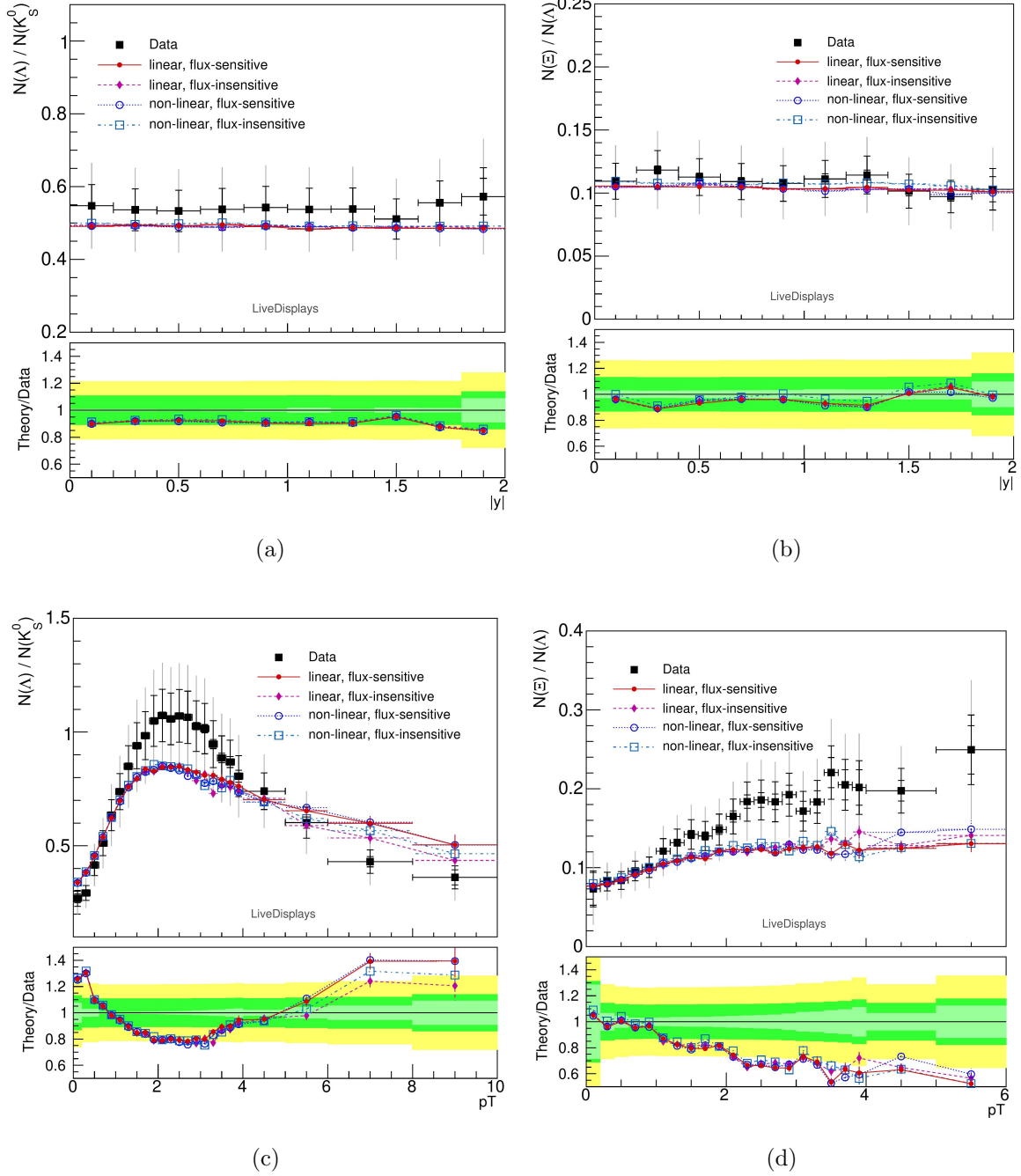


Figure 5.5. CMS data and PYTHIA simulations for non-single diffractive events are at $\sqrt{s} = 7$ TeV. (a)-(b) The ratio of yields of strange hadrons with respect to the absolute rapidity within $|y| < 2$. (c)-(d) The ratio of yields of strange hadrons with respect to the transverse momentum with no rapidity cuts made [25]. The models shown here are the different variations of the close packing model. A lifetime cut of $\tau_{max} = 10$ mm/c is made and no p_{\perp} cuts are applied to final state particles.

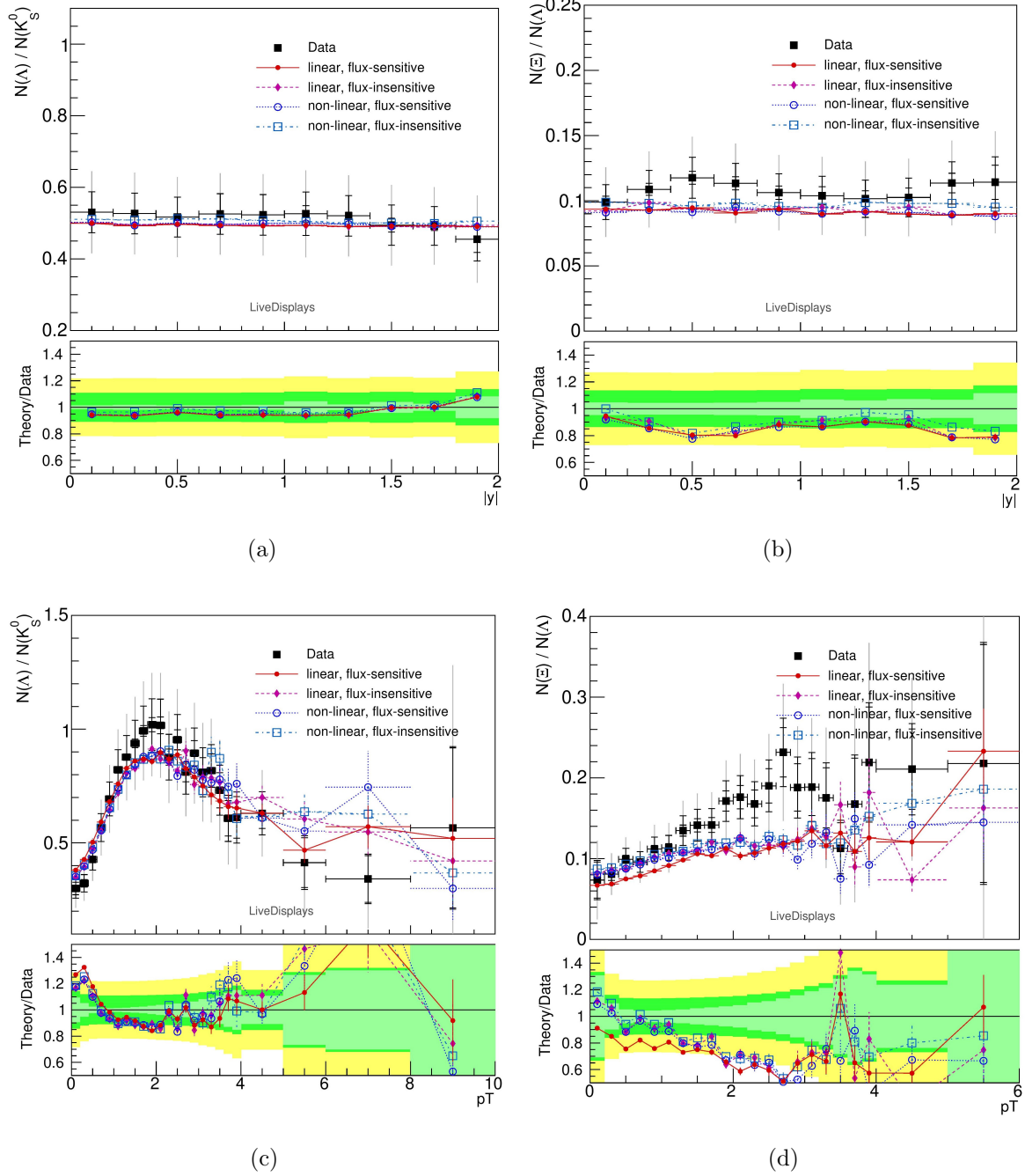


Figure 5.6. $\sqrt{s} = 900$ GeV non-single diffractive events. (a)-(b) The ratio of yields of strange hadrons with respect to the absolute rapidity within $|y| < 2$. (c)-(d) The ratio of yields of strange hadrons with respect to transverse momentum [25]. The models shown here are the different variations of the close packing model along with the CMS data. A lifetime cut of $\tau_{max} = 10$ mm/c is made and no p_{\perp} cuts are applied to final state particles.

5.4 Remaining Issues

Here we acknowledge shortcomings of the close packing model (that we are aware of) and other possible physics effects that could be at play, such as hadron rescattering. The primary issues we observed were overestimations of proton and kaon production relative to pions.

5.4.1 Baryon production

A consistent issue of all the models explored thus far is the overprediction of proton production. Even without any baryon enhancement through CR and close packing, the Monash tune overpredicts the proton to pion ratio of yields described by ALICE. However, the prediction given by the Monash tune shown in Figure 5.7 is consistent with that dictated by the e^+e^- collision data from LEP. Therefore, there appears to be an additional mechanism which is required in order to rectify this imbalance. The plots in Figure 5.7 show the ratio of baryons to mesons of equal strangeness content.

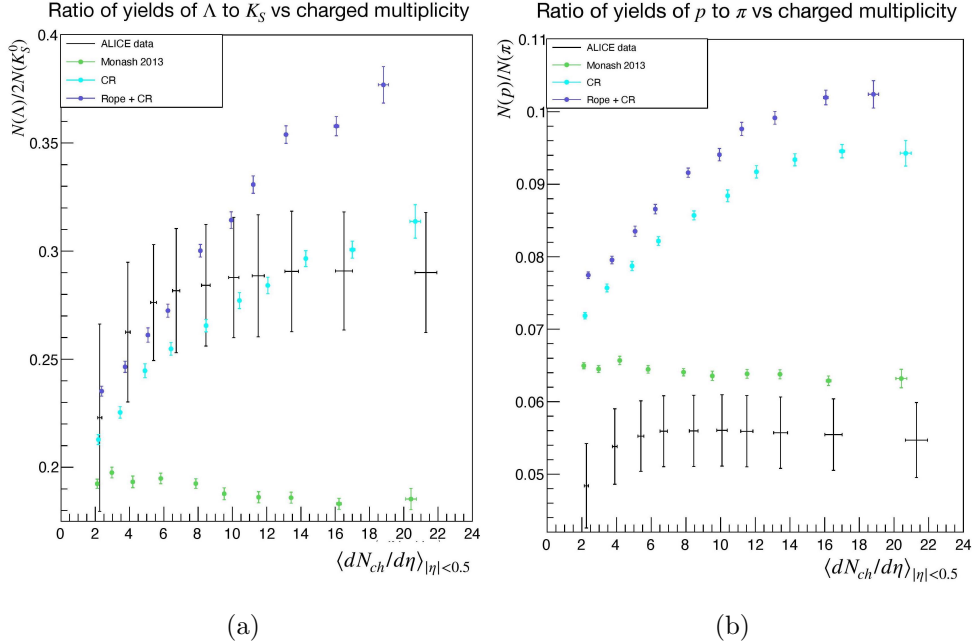


Figure 5.7. Baryon to meson ratios of existing models implemented in PYTHIA. (a) The ratio of Λ/K_S . (b) The ratio of p/π as a function of charged multiplicity. The PYTHIA simulations were inelastic events at $\sqrt{s} = 7$ TeV with no p_\perp or lifetime cuts applied.

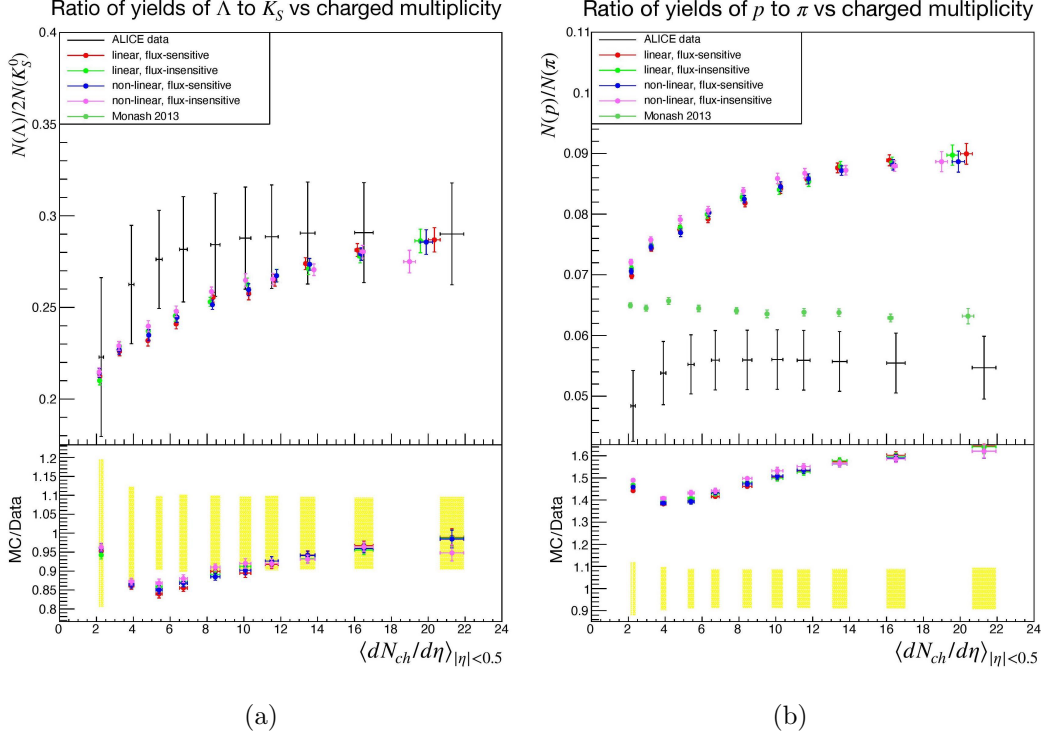


Figure 5.8. The close packing model variations of baryon to meson ratios. (a) The ratio of Λ/K_S . (b) The ratio of p/π as a function of charged multiplicity. The PYTHIA simulations were inelastic events at $\sqrt{s} = 7$ TeV with no p_{\perp} or lifetime cuts applied.

5.4.2 Hadron rescattering

With regard to the overestimation of the K_S/π and p/π ratios, one possible mechanism which could correct this is called hadron rescattering [28–30]. We have made a first crude trial by simply turning on the mechanism in order to get a qualitative notion of possible effects in conjunction with our close packing model. Figure 5.10 shows the results of the linearly-scaled flux-sensitive variation of the close packing model (see Appendix A for parameter values), alongside the close packing model with exact Casimir scaling with both hadron rescattering turned on and off. The parameters used for hadron rescattering were `HadronLevel:rescatter = on`, `Fragmentation:setVertices = on`, `Rescattering:impactModel = 1`, `Rescattering:opacity = 0.9` and `Rescattering:nearestNeighbours = off`.

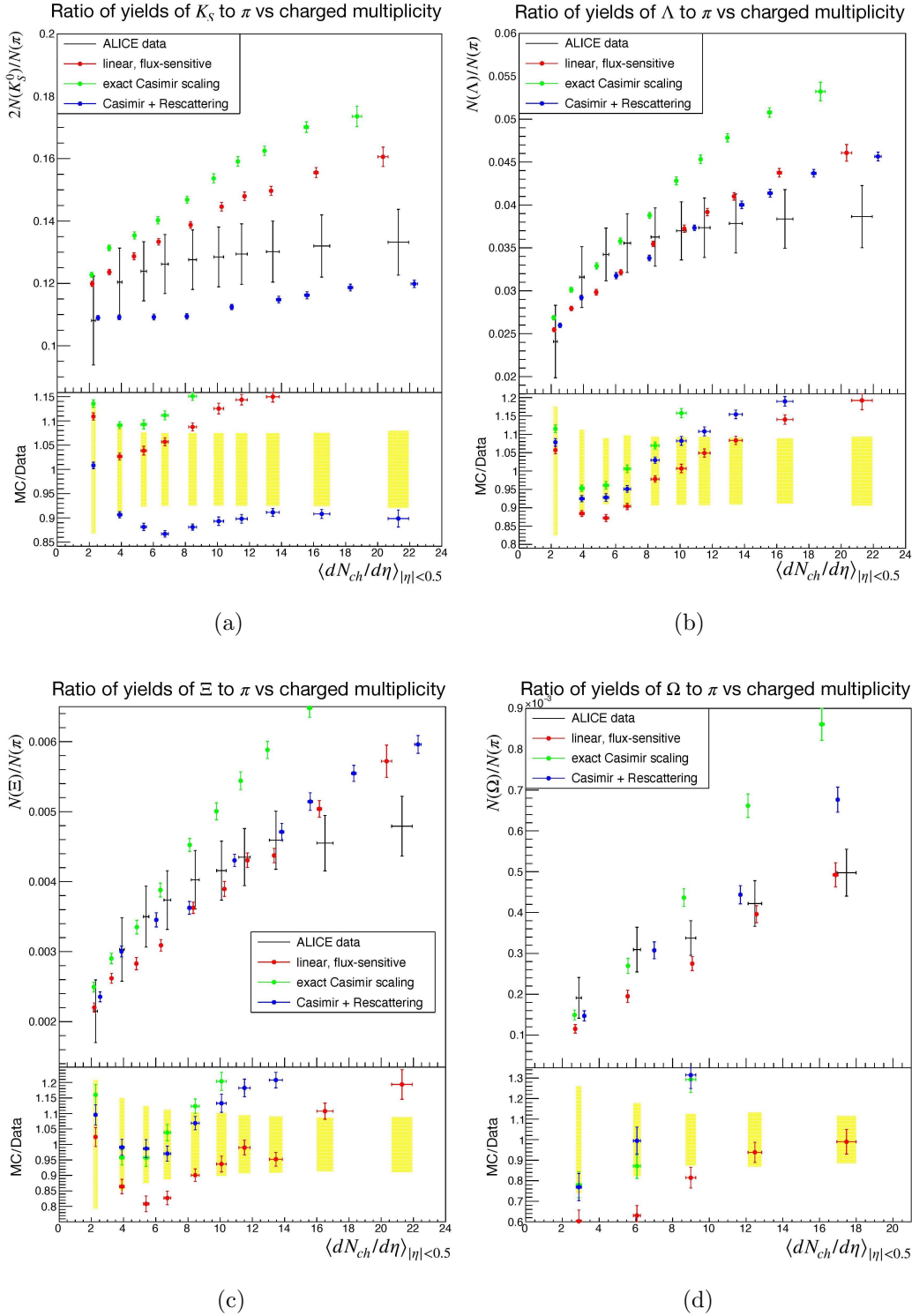


Figure 5.9. The ratio of strange hadrons to pions with respect to charged multiplicity, showing the effect of turning on hadron rescattering. All three implementations use $p_{\perp 0} = 0.6$, and they are inelastic events at $\sqrt{s} = 7$ TeV with no p_{\perp} or lifetime cuts applied.

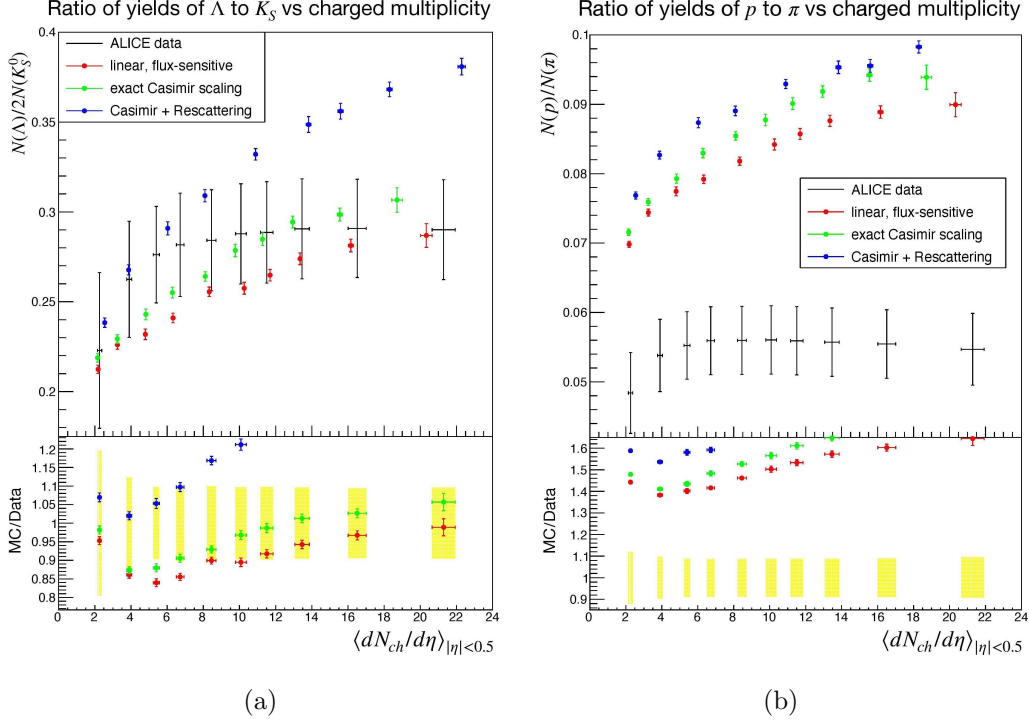


Figure 5.10. (a) The ratio of Λ/K_S and (b) shows the ratio of p/π as a function of charged multiplicity. These show baryon to meson ratios with model predictions including the linear flux-sensitive close packing model, and the close packing model following exact Casimir scaling with hadron rescattering turned on and off. In all three implementations, $p_{\perp 0} = 0.6$. All simulations were inelastic events at $\sqrt{s} = 7$ TeV with no p_{\perp} or lifetime cuts applied.

From these results alone, we can see that hadron rescattering does produce changes especially for kaon production in pp collisions. Importantly however, Figure 5.10 also shows that hadron rescattering results in large horizontal shifts of the mean multiplicities of the V0M multiplicity classes, which are indicative of significant changes in the multiplicity distribution. Thus retuning would be required in order to properly study the effects of hadron rescattering. Owing to the time constraints of the honours project, we did not pursue hadron rescattering in further depth, however our crude trial did demonstrate that this is certainly an area that merits future investigation.

6 Summary and Outlook

The results presented in Section 5 are encouraging, successfully resulting in a rise in strangeness as a function of charged multiplicity. The agreement with the ALICE data appears to be at least as good as for the more elaborate (and more computationally expensive) Rope model. We have also verified that overall features of the charged-particle modelling remains in good agreement with the CMS data [25–27] that was also used in Ref. [12].

Nevertheless there are several areas in which further improvements can be made to the model, which due to time constraints of the project have not yet been explored. These include both technical improvements as well as explorations of further physics effects.

Among technical issues, there are some possible modifications that could be made to the calculation of the rapidity pairs and the treatment of flux overall. In the current implementation (see Appendix C), gluon kinks are taken into consideration with the calculation of the rapidity pairs for both a standard $q\bar{q}$ string topology and for gluon loops. However, the gluons in junction topology string systems are ignored altogether. This was done for simplicity as the direction of colour flow is more difficult to map for junction topologies (see Figure 4.1), however for a more complete picture, gluon kinks in junction configurations should be accounted for.

Also regarding gluons, rather than being modelled by sharp kinks in the string as shown in Figure 2.1, in PYTHIA they are actually modelled by what are known as regions. As shown in Figure 6.1, the momentum of an intermediate gluon is spread across the string and creates a trapezoidal string topology instead of a sharp kink. The harder the gluon (i.e. the higher p_{\perp} the gluon has), the sharper the kink, as can be seen by comparing Figure 6.1a and 6.1b.

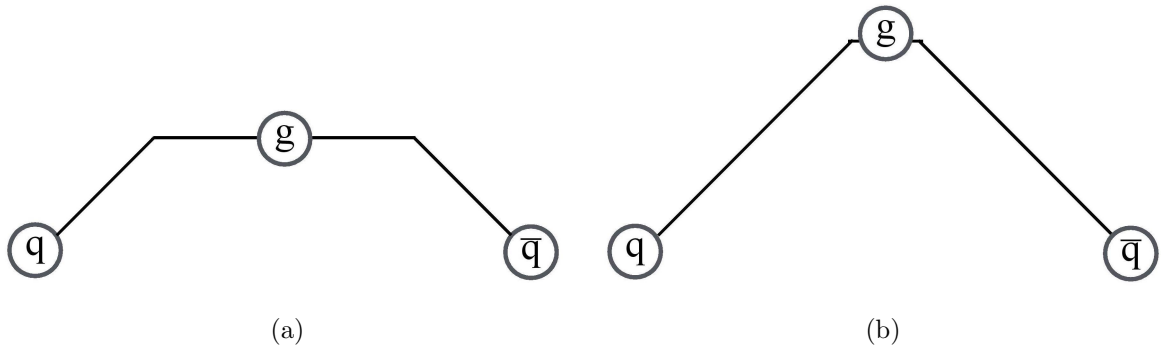


Figure 6.1. A $q\bar{q}$ string system where (a) has a soft gluon and (b) a hard gluon. Rather than the gluons being modelled by kinks, they are instead represented by regions.

Another future improvement would be to generalise the implementation to make the model applicable to e^+e^- collisions. Currently the implementation of close packing in PYTHIA determines string overlaps using rapidity with respect to the beam axis. As explained earlier, this is a physically reasonable measure to use for pp collisions as protons are a composition of coloured partons, thus due to beam remnants, this will result in the majority of the strings being orientated along the beam axis. This same assumption cannot be used for e^+e^- collisions as the majority of the strings will be orientated along jet axes which do not necessarily align with the beam axis. Thus the model could be generalised further to calculate rapidities along jet axes instead, though this has not been addressed thus far in our implementation.

Among exploration of further physics effects, in particular we regard a closer study of the interplay between colour reconnections, close packing, and hadronic rescattering as interesting to pursue. A study of close-packing effects on heavy-flavour fragmentation would likewise be both interesting and timely, especially in view of new results from over the past year. The QCD CR model can predict the Λ_c/D^0 ratio [31, 32] as well as what is known as “bottom asymmetries” [33]. However CR alone cannot describe the Ξ_c/D^0 ratio [34] which requires a strangeness increase, and hence it would be worth exploring the effects of close packing on such observables.

Nonetheless, the results are already promising, having successfully achieved strangeness enhancement with respect to charged multiplicity, and close packing is a mechanism that certainly warrants further investigation.

References

- [1] ALICE collaboration, *Enhanced production of multi-strange hadrons in high-multiplicity proton-proton collisions*, *Nature Phys.* **13** (2017) 535 [[1606.07424](#)].
- [2] T. Sjöstrand, S. Mrenna and P. Z. Skands, *A Brief Introduction to PYTHIA 8.1*, *Comput. Phys. Commun.* **178** (2008) 852 [[0710.3820](#)].
- [3] T. Sjöstrand, S. Ask, J. R. Christiansen, R. Corke, N. Desai, P. Ilten et al., *An introduction to PYTHIA 8.2*, *Comput. Phys. Commun.* **191** (2015) 159 [[1410.3012](#)].
- [4] P. Skands, S. Carrazza and J. Rojo, *Tuning PYTHIA 8.1: the Monash 2013 Tune*, *Eur. Phys. J. C* **74** (2014) 3024 [[1404.5630](#)].
- [5] N. Fischer and T. Sjöstrand, *Thermodynamical String Fragmentation*, *JHEP* **01** (2017) 140 [[1610.09818](#)].
- [6] B. Andersson, *The Lund model*, vol. 7. Cambridge University Press, 7, 2005.
- [7] B. Andersson, G. Gustafson, G. Ingelman and T. Sjöstrand, *Parton fragmentation and string dynamics*, *Physics Reports* **97** (1983) 31.
- [8] E. Eichten, K. Gottfried, T. Kinoshita, K. D. Lane and T.-M. Yan, *Charmonium: The Model*, *Phys. Rev. D* **17** (1978) 3090.
- [9] G. S. Bali and K. Schilling, *Static quark - anti-quark potential: Scaling behavior and finite size effects in $SU(3)$ lattice gauge theory*, *Phys. Rev. D* **46** (1992) 2636.
- [10] P. Skands, *Introduction to QCD*, in *Theoretical Advanced Study Institute in Elementary Particle Physics: Searching for New Physics at Small and Large Scales*, 7, 2012, DOI [[1207.2389](#)].
- [11] T. Sjöstrand and V. A. Khoze, *On Color rearrangement in hadronic $W^+ W^-$ events*, *Z. Phys. C* **62** (1994) 281 [[hep-ph/9310242](#)].
- [12] J. R. Christiansen and P. Z. Skands, *String Formation Beyond Leading Colour*, *JHEP* **08** (2015) 003 [[1505.01681](#)].

- [13] T. Sjöstrand and M. van Zijl, *A Multiple Interaction Model for the Event Structure in Hadron Collisions*, *Phys. Rev. D* **36** (1987) 2019.
- [14] J. Schwinger, *On gauge invariance and vacuum polarization*, *Phys. Rev.* **82** (1951) 664.
- [15] G. C. Nayak, *Non-perturbative quark-antiquark production from a constant chromo-electric field via the Schwinger mechanism*, *Phys. Rev. D* **72** (2005) 125010 [[hep-ph/0510052](#)].
- [16] B. Andersson, G. Gustafson and B. Söderberg, *A Probability Measure on Parton and String States*, *Nucl. Phys. B* **264** (1986) 29.
- [17] T. Sjöstrand and P. Z. Skands, *Baryon number violation and string topologies*, *Nucl. Phys. B* **659** (2003) 243 [[hep-ph/0212264](#)].
- [18] A. Buckley, J. Butterworth, D. Grellscheid, H. Hoeth, L. Lönnblad, J. Monk et al., *Rivet user manual*, *Comput. Phys. Commun.* **184** (2013) 2803 [[1003.0694](#)].
- [19] C. Flensburg, G. Gustafson and L. Lönnblad, *Inclusive and Exclusive Observables from Dipoles in High Energy Collisions*, *JHEP* **08** (2011) 103 [[1103.4321](#)].
- [20] T. Pierog, I. Karpenko, J. M. Katzy, E. Yatsenko and K. Werner, *EPOS LHC: Test of collective hadronization with data measured at the CERN Large Hadron Collider*, *Phys. Rev. C* **92** (2015) 034906 [[1306.0121](#)].
- [21] C. Bierlich, *Rope Hadronization and Strange Particle Production*, *EPJ Web Conf.* **171** (2018) 14003 [[1710.04464](#)].
- [22] G. S. Bali, *Casimir scaling of $SU(3)$ static potentials*, *Phys. Rev. D* **62** (2000) 114503 [[hep-lat/0006022](#)].
- [23] C. Bierlich, G. Gustafson, L. Lönnblad and A. Tarasov, *Effects of Overlapping Strings in pp Collisions*, *JHEP* **03** (2015) 148 [[1412.6259](#)].
- [24] ALICE collaboration, *Production of $K^*(892)^0$ and $\phi(1020)$ in pp collisions at $\sqrt{s} = 7$ TeV*, *Eur. Phys. J. C* **72** (2012) 2183 [[1208.5717](#)].
- [25] CMS collaboration, *Strange Particle Production in pp Collisions at $\sqrt{s} = 0.9$ and 7 TeV*, *JHEP* **05** (2011) 064 [[1102.4282](#)].

- [26] CMS collaboration, *Transverse-momentum and pseudorapidity distributions of charged hadrons in pp collisions at $\sqrt{s} = 7$ TeV*, *Phys. Rev. Lett.* **105** (2010) 022002 [[1005.3299](#)].
- [27] CMS collaboration, *Charged Particle Multiplicities in pp Interactions at $\sqrt{s} = 0.9, 2.36, \text{ and } 7$ TeV*, *JHEP* **01** (2011) 079 [[1011.5531](#)].
- [28] Y. Kanakubo, Y. Tachibana and T. Hirano, *Interplay between core and corona components in high-energy nuclear collisions*, [2108.07943](#).
- [29] K. Werner, A. G. Knospe, C. Markert, B. Guiot, I. Karpenko, T. Pierog et al., *Resonance production in high energy collisions from small to big systems*, *EPJ Web Conf.* **171** (2018) 09002 [[1812.06330](#)].
- [30] C. Bierlich, T. Sjöstrand and M. Utheim, *Hadronic rescattering in pA and AA collisions*, *Eur. Phys. J. A* **57** (2021) 227 [[2103.09665](#)].
- [31] ALICE collaboration, *Measurement of prompt D^0 , Λ_c^+ , and $\Sigma_c^{0,++}$ (2455) production in pp collisions at $\sqrt{s} = 13$ TeV*, [2106.08278](#).
- [32] ALICE collaboration, *Λ_c^+ production in pp and in p-Pb collisions at $\sqrt{s_{NN}}=5.02$ TeV*, *Phys. Rev. C* **104** (2021) 054905 [[2011.06079](#)].
- [33] LHCb collaboration, *Observation of a $\Lambda_b^0 - \bar{\Lambda}_b^0$ production asymmetry in proton-proton collisions at $\sqrt{s} = 7$ and 8 TeV*, *JHEP* **10** (2021) 060 [[2107.09593](#)].
- [34] ALICE collaboration, *Measurement of the cross sections of Ξ_c^0 and Ξ_c^+ baryons and branching-fraction ratio $BR(\Xi_c^0 \rightarrow \Xi^- e^+ \nu_e)/BR(\Xi_c^0 \rightarrow \Xi^- \pi^+)$ in pp collisions at 13 TeV*, [2105.05187](#).

Appendices

A Model Parameters

Table A1: Parameter values used in Monash 2013 tune, CR Mode 2 and the rope model.

Parameter	Monash	Mode 2	Rope
StringPT:sigma	= 0.335	= 0.335	= 0.335
StringZ:aLund	= 0.68	= 0.36	= 0.68
StringZ:bLund	= 0.98	= 0.56	= 0.98
StringFlav:probQQtoQ	= 0.081	= 0.078	= 0.081
StringFlav:probStoUD	= 0.217	= 0.2	= 0.217
StringFlav:probQQ1toQQ0	= 0.0275	= 0.0275	= 0.0275
StringFlav:probQQ1toQQ0join	= 0.5, 0.7, 0.9, 1.0	= 0.0275, 0.0275, 0.0275, 0.0275	= 0.5, 0.7, 0.9, 1.0
MultiPartonInteractions:pT0Ref	= 2.28	= 2.15	= 2.15
BeamRemnants:remnantMode	= 0	= 1	= 1
BeamRemnant:saturation	-	= 5	= 5
ColourReconnection:mode	= 0	= 1	= 1
ColourReconnection:allowDoubleJunRem	= on	= off	= off
ColourReconnection:m0	-	= 0.3	= 0.3
ColourReconnection:allowJunctions	-	= on	= on
ColourReconnection:junctionCorrection	-	= 1.2	= 1.2
ColourReconnection:timeDilationMode	-	= 2	= 2
ColourReconnection:timeDilationPar	-	= 0.18	= 0.18

Parameter	Monash	Mode 2	Rope
Ropewalk:doShoving	= off	= off	= on
Ropewalk:tInit	-	-	= 1.5
Ropewalk:deltat	-	-	= 0.05
Ropewalk:tShove	-	-	= 0.1
Ropewalk:gAmplitude	-	-	= 0
Ropewalk:doFlavour	= off	= off	= on
Ropewalk:r0	-	-	= 0.5
Ropewalk:m0	-	-	= 0.2
Ropewalk:beta	-	-	= 0.1
PartonVertex:setVertex	= off	= off	= on
PartonVertex:protonRadius	-	-	= 0.7
PartonVertex:emissionWidth	-	-	= 0.1

Table A2: Parameter values used for the close packing model variations.

Parameter	Flux-sensitive		Flux-insensitive	
	Linear	Exponential	Linear	Exponential
StringPT:sigma	= 0.335	= 0.335	= 0.335	= 0.335
StringZ:aLund	= 0.36	= 0.36	= 0.36	= 0.36
StringZ:bLund	= 0.56	= 0.56	= 0.56	= 0.56
StringFlav:probQQtoQ	= 0.078	= 0.078	= 0.078	= 0.078
StringFlav:probStoUD	= 0.2	= 0.2	= 0.2	= 0.2
StringFlav:probQQ1toQQ0join	= 0.5, 0.5, 0.0275, 0.0275	= 0.5, 0.5, 0.0275, 0.0275	= 0.5, 0.5, 0.0275, 0.0275	= 0.5, 0.5, 0.0275, 0.0275
MultiPartonInteractions:pT0Ref	= 2.2	= 2.2	= 2.2	= 2.2
BeamRemnants:remnantMode	= 1	= 1	= 1	= 1
BeamRemnant:saturation	= 5	= 5	= 5	= 5
ColourReconnection:mode	= 1	= 1	= 1	= 1
ColourReconnection:allowDoubleJunRem	= off	= off	= off	= off
ColourReconnection:m0	= 0.3	= 0.3	= 0.3	= 0.3
ColourReconnection:allowJunctions	= on	= on	= on	= on
ColourReconnection:junctionCorrection	= 1.0	= 1.0	= 1.0	= 1.0
ColourReconnection:timeDilationMode	= 2	= 2	= 2	= 2
ColourReconnection:timeDilationPar	= 0.18	= 0.18	= 0.18	= 0.18
ClosePacking:allow	= on	= on	= on	= on
ClosePacking:expNSP	= 0.5	= 0.35	= 0.5	= 0.13
ClosePacking:PT0	= 0.6	= 0.6	= 0.6	= 0.6
ClosePacking:tension	= 0.16	= 0.25	= 0.116	= 1.0
ClosePacking:tensionRatio	= 0.5	= 0.5	= 1.0	= 1.0

B Diquark to quark probability

`StringFlav:ProbQQtoQ` is a global probability and thus takes a more complicated form of modification than the other probabilities in the `StringFlav` class. The probability of diquarks to quarks is given by Equation (B.1) [23]. Here we assume u and d are treated on equal footing with equal probabilities.

$$P(qq : q) = \frac{\sum_{qq_s} \mathcal{P}_{qq_s}}{\sum_q \mathcal{P}_q} = \alpha \frac{\mathcal{P}_{ud0}}{\mathcal{P}_u}. \quad (\text{B.1})$$

The variable α is given by Equation (B.2), whereby $\mathcal{P}_s = \rho\mathcal{P}_u$, $\mathcal{P}_{ud1} = 3y\mathcal{P}_{ud0}$ and $\mathcal{P}_{us1} = x\rho\mathcal{P}_{ud1}$, etc. The parameters ρ, x and y are given in Table B1.

Table B1: Parameter symbols and their corresponding PYTHIA parameters.

Symbol	PYTHIA Parameters
ρ	probStoUD
x	probSQtoQQ
y	probQQ1toQQ0

$$\alpha = \frac{1 + 2x\rho + 9y + 6x\rho y + 3yx^2\rho^2}{2 + \rho}. \quad (\text{B.2})$$

We have reparametrised the form of $P'(qq : q)$ given in [23] in order to not assume the dependence on κ_{eff} of $\mathcal{P}_{ud0}/\mathcal{P}_u$. This reparametrisation is given in Equation (B.4), where $\tilde{\alpha}$ is given by Equation (B.2) and takes into account the modifications due to an effective string tension on the probabilities ρ, x and y . The variable R_κ^{QQ} is given by (B.3), and scales with the parameter f_{QQ} which is fit to data. As $f_{QQ} \rightarrow 1$, $\mathcal{P}_{ud0}/\mathcal{P}_u$

scales as per `probStoUD`, whereas when $f_{QQ} \rightarrow 0$, $\mathcal{P}_{ud0}/\mathcal{P}_u$ becomes insensitive to changes in an effective string tension.

$$R_{\kappa}^{QQ} = 1 + f_{QQ}^2 \left(\frac{\kappa_{eff}}{\kappa_0} - 1 \right). \quad (\text{B.3})$$

$$P'(qq : q) = \tilde{\alpha} \left(\frac{P(qq : q)}{\alpha} \right)^{\frac{1}{R_{\kappa}^{QQ}}}. \quad (\text{B.4})$$

C PYTHIA code

C.1 rapidityPairs in HadronLevel.cc

```
// Extract rapidity pairs of string pieces.

vector< vector< pair<double, double> > > HadronLevel::rapidityPairs(
    Event& event) {

    // Loop over all string systems in the event.
    vector< vector< pair<double, double> > > rapPairs;
    for (int iSub = 0; iSub < int(colConfig.size()); iSub++) {
        vector< pair<double, double> > rapsNow;
        vector<int> iPartons = colConfig[iSub].iParton;

        // Special treatment for junction systems.
        if (colConfig[iSub].hasJunction) {
            vector<double> yLegQ;
            vector<double> yLegQbar;
            vector<int> yType;

            // Pick smallest and largest rapidity parton.
            for (int iP = 0; iP < int(iPartons.size()); iP++) {
                int iQ = iPartons[iP];
```

```

if (iQ < 0) continue;
if (event[iQ].id() == 21) continue;
// Does not account for gluons. Modification to be made in future.
double yNow = yMax(event[iQ], MTINY);
// Sort quark and antiquark cases seperately.
if (event[iQ].id() < 0) yLegQbar.push_back(yNow);
else yLegQ.push_back(yNow);
}

// Order quarks/antiquarks in order ascending rapidity.
if (yLegQ.size() > 0) sort(yLegQ.begin(), yLegQ.end());
if (yLegQbar.size() > 0) sort(yLegQbar.begin(), yLegQbar.end());

// Simple junction systems.
if (yLegQ.size() == 3) {
    rapsNow.push_back(make_pair(yLegQ[0], yLegQ[1]));
    rapsNow.push_back(make_pair(yLegQ[2], yLegQ[1]));
}
else if (yLegQbar.size() == 3) {
    rapsNow.push_back(make_pair(yLegQbar[1], yLegQbar[0]));
    rapsNow.push_back(make_pair(yLegQbar[1], yLegQbar[2]));
}

// Junction-Antijunction systems.
else if (yLegQ.size() == 2 && yLegQbar.size() == 2) {
    //  $q_0 \rightarrow q_1 \leftarrow qbar_0 \rightarrow qbar_1$ .
    double minQ = min(yLegQ[0], yLegQ[1]);
    double minQbar = min(yLegQbar[0], yLegQbar[1]);
    if (minQ < minQbar) {
        rapsNow.push_back(make_pair(yLegQ[0], yLegQ[1]));
        rapsNow.push_back(make_pair(yLegQbar[0], yLegQ[1]));
        rapsNow.push_back(make_pair(yLegQbar[0], yLegQbar[1]));
    }
    //  $qbar_0 \leftarrow qbar_1 \rightarrow q_0 \leftarrow q_1$ .

```

```

    else {
        rapsNow.push_back(make_pair(yLegQbar[1], yLegQbar[0]));
        rapsNow.push_back(make_pair(yLegQbar[1], yLegQ[0]));
        rapsNow.push_back(make_pair(yLegQ[1], yLegQ[0]));
    }
}

// Return error message if junction is none of the above cases.
else {
    infoPtr->errorMsg("Error_in_HadronLevel::rapidityPairs:_
                    "Could_not_determine_junction_type.");
}

// Normal strings. For closed gluon loop include first-last pair.
} else {
    int size = int(iPartons.size());
    int end = size - (colConfig[iSub].isClosed ? 0 : 1);
    for (int iP = 0; iP < end; iP++) {
        int i1 = iPartons[iP];
        int i2 = iPartons[(iP+1)%size];
        double y1 = yMax(event[i1], MTINY);
        double y2 = yMax(event[i2], MTINY);
        rapsNow.push_back(make_pair(y1, y2));
    }
}
rapPairs.push_back(rapsNow);
}
// Done.
return rapPairs;
}

```

C.2 kappaEffectiveRatio in StringFragmentation.cc

```

// Implemented in close packing to calculate the change in the

```

```

// string tension due to surrounding strings.
// kappaEffRatio returns the ratio of kappaEff to kappa0.
// Note: optional exponential scaling is not taken into account here and
// instead applied afterwards.

double StringFragmentation::kappaEffRatio(StringSystem& systemNow,
StringEnd end, vector< vector< pair<double, double> > >& rapPairs,
double mRem, Event& event) {

// Get temporary hadron momentum.
// Elaborate check for thermal model.
Vec4   pHad      = Vec4(0., 0., 0., -1.);
double phi       = 2.0 * M_PI * rndmPtr->flat();
double mult      = -1.0;
int     nTryMax  = 100;
double multStep  = 5.0 / ((double)nTryMax/2);
double multNow   = 1.0 + multStep;
for (int i = 1; i <= nTryMax; i++) {
    pHad = end.kinematicsHadronTmp(systemNow, mRem, phi, mult);
    // If valid momentum found, done.
    if (pHad.e() > 0.0) break;
    // Set mult as multiplicative factor. Alternate between adding and
    // subtracting multStep.
    mult = 1.0;
    if (i%2 == 0) {
        mult *= multNow;
        multNow += multStep;
    } else mult /= multNow;
}

// In case of failure, use remnant momentum.
if (pHad.e() < 0.0) pHad = pRem;

```

```

// Boost to JRF.
if (hasJunction) {
    pHad.rotbst(MfromJRF);
}

// Extract pT2 of hadron.
double pT2Had    = pHad.pT2();
// Now loop through the list of rapidity pairs and count strings
    // sitting at the hadron rapidity.
Particle hadron = Particle();
hadron.p(pHad); hadron.m(pHad.mCalc());
double yHad = hadron.y();

// p and q have same and opposite flux as fragmenting
// string respectively.
// Start p at -1 to subtract off current string.
int p = -1;
int q = 0;
// Flux direction of current string.
bool fluxDirPos = false;
if (event[posEnd.iEnd].y() < event[negEnd.iEnd].y()) fluxDirPos = true;
if (event[posEnd.iEnd].colType() < 0) fluxDirPos = !fluxDirPos;
// Find rapidity overlaps.
for (int iSub = 0; iSub < int(rapPairs.size()); iSub++) {
    vector< pair<double, double> > pairNow = rapPairs[iSub];
    for (int iPair = 0; iPair < int(pairNow.size()); iPair++) {
        double y1;
        double y2;
        if (fluxDirPos) {
            y1 = pairNow[iPair].first;
            y2 = pairNow[iPair].second;
        } else {
            y1 = pairNow[iPair].second;

```

```

        y2 = pairNow[iPair].first;
    }

    if ( (y1 < y2) && (y1 < yHad) && (yHad < y2) ) {
        p++;
    } else if ( (y2 < y1) && (y2 < yHad) && (yHad < y1) ) {
        q++;
    }

}

}

// Number of strings effective contribution taking pT into account.
double nNSPEff = closePackingTension * (p + closePackingTensionRatio*q)
    / (1.0 + pT2Had / closePackingPT20);

// Add back current string.
return nNSPEff + 1.0;
}

```

C.3 Reinitialisation of Probabilities in FragmentationFlavZpT.cc

```

void StringFlav::reinit(double kappaRatio) {

    double kappaRatioEff = pow(kappaRatio, 2*exponentNSP);
    double kappaInvRatio = 1. / kappaRatioEff;

    // Altered probabilities with close packing.
    probStoUD = pow(probStoUDSav, kappaInvRatio);
    probSQtoQQ = pow(probSQtoQQSav, kappaInvRatio);
    probQQ1toQQ0 = pow(probQQ1toQQ0Sav, kappaInvRatio);

    double alphaQQ = 1. + 2. * probSQtoQQ * probStoUD + 9. * probQQ1toQQ0

```

```

+ 6. * probSQtoQQ * probQQ1toQQ0 * probStoUD
+ 3. * probQQ1toQQ0 * pow(probSQtoQQ * probStoUD, 2.0);
alphaQQ *= 1. / (2 + probStoUD);
// Diquark scaling power controlled by closePackingFacQQ.
double kappaRatioQQ = 1. + closePackingFacQQ2 * (kappaRatioEff - 1.);
double kappaInvRatioQQ = 1. / kappaRatioQQ;
probQQtoQ = alphaQQ * pow( (probQQtoQSav/alphaQQSav ), kappaInvRatioQQ);

// Parameters derived from above.
probQandQQ = 1. + probQQtoQ;
probQandS = 2. + probStoUD;
probQandSinQQ = 2. + probSQtoQQ * probStoUD;
probQQ1corr = 3. * probQQ1toQQ0;
probQQ1corrInv = 1. / probQQ1corr;
probQQ1norm = probQQ1corr / (1. + probQQ1corr);

// reinitialisation of other values dependent on
// these modified probabilities
...

```

D ALICE Analysis

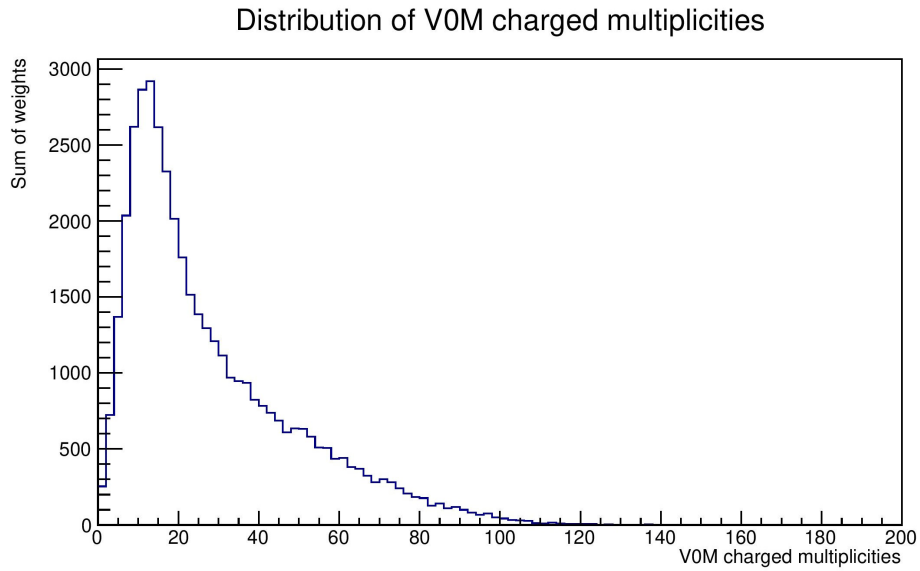
In the RIVET analysis [18] provided by the ALICE collaboration, primary particles are such that none of the ancestor particles are also primary. This means that the decay products of a given primary particle is not also counted as primary. The list of particles considered primary (along with their antiparticle counterparts) are; μ , e , γ , n , p , ν_e , ν_μ , ν_τ , π , K^+ , K_L^0 , K_S^0 , Λ , Σ^- , Σ^+ , Ξ^0 , Ξ^- , and Ω ,

In order to study the dependence on charged multiplicity, we look to the V0M multiplicity and its correlation to the midrapidity charged multiplicity. The V0M multiplicity is the the charged particle multiplicity in the forward detectors, spanning the

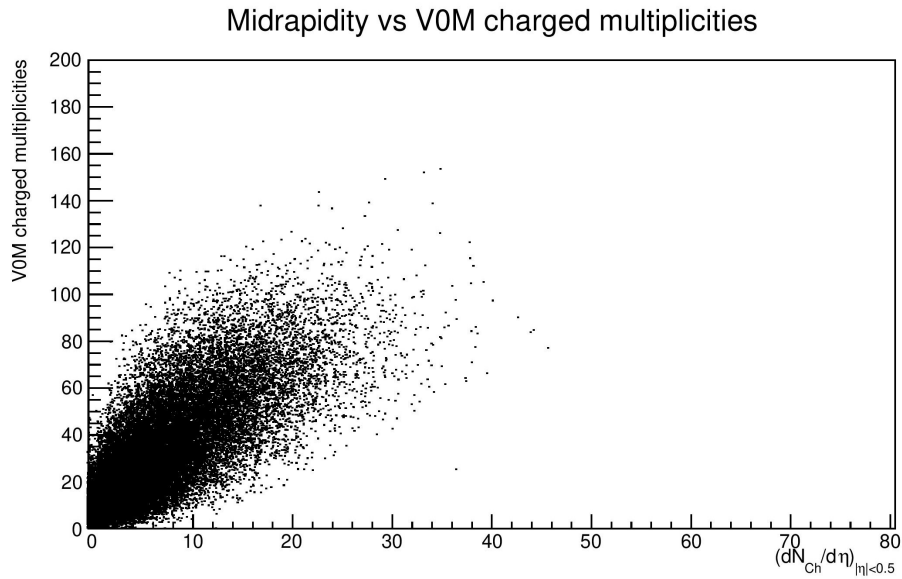
pseudorapidities $2.8 < \eta < 5.1$ and $-3.7 < \eta < -1.7$. It includes all final state charged particles, not primary particles in particular. This means that in the simulations, no lifetime cuts are made. However, the midrapidity charged multiplicity counts only primary charged particles. The event classes are determined using centrality bins which decrease progressively with $\langle dN_{ch}/d\eta \rangle_{|\eta| < 0.5}$.

Figure D.1a shows the distribution of V0M multiplicities. The range of V0M multiplicities used for each event class is determined by the statistics of this distribution, whereby the percentiles defining the classes are $\{0.30, 0.50, 0.60, 0.70, 0.80, 0.85, 0.90, 0.95, 0.99, 1\}$. Due to the low statistics of omega baryons, a smaller number of event classes are used and given by the percentiles $\{0.50, 0.70, 0.85, 0.95, 1\}$.

In order to examine the correlation between the V0M and midrapidity multiplicities (or more specifically, multiplicities in the midpseudorapidity of $|\eta| < 0.5$), the distribution given in Figure D.1b is used. A given event class spans a range of V0M multiplicities determined by the percentiles described above. Thus, in order to determine the corresponding midrapidity multiplicity, the mean of the Figure D.1b distribution within the given V0M range is used.



(a)



(b)

Figure D.1. (a) An example of a distribution of the V0M charged particle multiplicities, and (b) the corresponding scatter plot of the V0M charged particle multiplicities vs the midrapidity ($|\eta| < 0.5$) primary charged particle multiplicities.